Towards a microfluidic device for magnetic isolation and encapsulation of circulating tumour cells

Koot, J.M.

Award date:
2019

EINDHOVEN UNIVERSITY OF TECHNOLOGY

Towards a microfluidic device for magnetic isolation and encapsulation of circulating tumour cells

Master Thesis: TU/e Microsystems - Erasmus UMC

March 13th 2019 - December 2nd 2019

Student	J.M. Koot, 0844336
Supervisor	Prof. Dr. Ir. J.M.J. den Toonder, Microsystems, TU Eindhoven
Committee	Prof. Dr. J.W.M. Martens, Medical Oncology, Erasmus UMC Rotterdam
	Dr. R. Luttge, Microsystems, TU Eindhoven
Advisory	Dr. J. Kraan, Medical Oncology, Erasmus UMC Rotterdam

TU/e - Mechanical Engineering - Microsystems

Eindhoven, November 22, 2019

Abstract

Metastasis is the main cause of cancer related deaths, rather than the primary tumour. Tumour cells that escape from the primary tumour and enter the blood vessels, to circulate throughout the body are called circulating tumour cells (CTCs). CTC concentrations in patients are extremely low with usually one to ten CTCs for every millilitre of whole blood. CTCs that stem from epithelial tissue express epithelial cell adhesion molecules (EpCAM). Commercially available CellSearch technology currently uses EpCAM antibody ferrofluids to isolate and count CTC concentrations in patients to make a prognosis for the chances of survival of the patient.

Ongoing research at TU/e's Microsystems group aims to establish a microfluidic system that can do three actions in tandem: first, the isolation of CTCs, followed by the encapsulation of these cells in Matrigel beads and subsequently establishing a three-dimensional culture inside these beads. These cultures could then be used for medicine research or for patient-specific diagnostics, possibly paving a new road to personalized cancer medicine. Diagnostics and prognostics by CTC culture analysis would also come with the benefit of being significantly less physically straining than surgical tissue removal and analysis, while also targeting cells that are in the process of metastasising rather than the main tumour.

This research succeeded in establishing a microfluidic isolation chamber that could be mounted onto and detached from a magnetic platform that was able to capture and release most of the MCF-7 cell line tumour cells spiked into medium at relatively high flowrates (0.1 to 1 mL/min) by using the same ferrofluid and capture enhancer as used in the CellSearch technology, thereby establishing the first step of a microfludic CTC capture and cell culture analysis device.

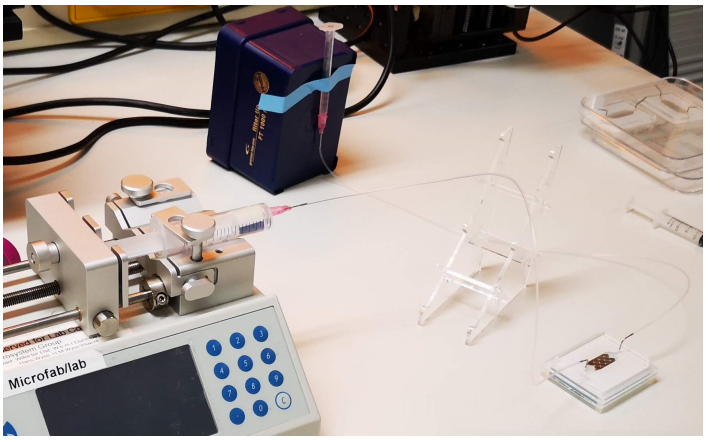

Figure 0.1: *Syringe pump withdrawing MCF-7 cell suspension through the isolation chamber.*

Lists of symbols and abbreviations

Symbol	Physical quantity	Base units	Abbreviation
A	Channel cross-section	Square meters	[m^2]
B	Magnetic flux density	Tesla	[T]
C	Particle concentration	Per cubic meter	[m^{-3}]
Ca	Capillary number	Dimensionless	[-]
d	Diameter	Meter	[m]
F	Force	Newton	[N]
h	Width	Meter	[m]
Q	Flowrate	Cubic meter per second	[m^3/s]
r	Radius	Meter	[m]
u	Velocity	Meter per second	[m/s]
V	Volume	Cubic meter	[m^3]
w	Width	Meter	[m]
We	Weber number	Dimensionless	[-]
x	Position	Meter	[m]
y	Position	Meter	[m]
z	Position	Meter	[m]
γ	Surface tension	Joules per square meter	[N/m]
η	Dynamic viscosity	Pascal second	[Pas]
μ_0	Magnetic permeability of a vacuum	Henry per meter	[H/m]
ρ	Density	Kilogram per cubic meter	[kg/m^3]
χ	Magnetic susceptibility	Dimensionless	[-]

Symbol	Meaning
act	actuation/action
c	channel
$drag$	(Stokes)drag
in	inner
out	outer
tip	tip of nozzle
x	x-direction
y	y-direction
z	z-direction

Abbreviation	Definition
CTC	Circulating tumour cell
DI	De-ionized (water)
EpCAM	Epithelial cell adhesion molecule
EpCAM+	Expressing EpCAM
EpCAM-	Expressing no EpCAM
MCF-7	Michigan Cancer Foundation-7
MIMO	Multiple inflow, multiple outflow
PDMS	Polydimethylsiloxane
PMMA	Polymethylmethacrylate
TC	Tumour cell
WBC	White blood cell

Contents

1 Introduction

Cancer has been a major cause of death in human history. However, as the average life expectancy of the population increases due to healthier habits, better healthcare and safer environments, cancer's contribution to mortality increases as it is a disease that is ever more likely to manifest itself with increasing age. A cause for this is the gradual damaging of DNA sequences in the cell, leading to different behaviour of these cells when compared to their predecessors. Usually, malfunctioning cells are killed by the human body itself in a process called apoptosis. When a patient suffers from cancer, malfunctioning cells are not killed but they are able to keep proliferating uncontrollably. A lump of these uncontrollably growing malfunctioning cells is called a tumour. Tumours by themselves are not the leading cause of death for cancer. Most cancer related deaths are caused by the spreading of tumour cells from the initial (primary) tumour to other vital places inside the body. This spreading of tumour cells is called metastasis.

The process of metastasis [Sleeboom et al., 2018] starts with tumour cells escaping from the primary tumour, migrating into the blood vessels. This is called invasion. The tumour cell then enters and passes the blood vessel wall, which is called intravasation. The tumour cell is now inside the blood circulation system, leading to the term circulating tumour cell (CTC). Whenever multiple CTCs survive for long enough inside the blood vessel, it is only a matter of time before a CTC exits the blood system (extravasation) and takes root someplace else in the body where the tumour cell can start proliferating and cause a new tumour at this so-called metastatic site.

Since metastasis is the leading cause of cancer deaths, it is evident that further exploration of this subtopic in cancer research is vital to improve the quality of life and improve the prognosis of patients. In vitro experiments on cancer cells have been executed in petri dishes. However, the rigidity and flatness of this environment are hardly comparable to the in vivo situation. For this reason, several attempts are being made to produce in vitro cultures from CTCs extracted from human patients in microfluidic chips by representing the tumour microenvironment as best as possible.

Usually, symptoms of cancer can be recognized by the patient in everyday life or by a doctor during a procedural screening. Well-known symptoms of cancer include unintended weight-loss and tiredness. When one or several cancer symptoms have been recognized, diagnostic procedures follow in order to confirm the presence of cancer. Blood tests, CT scans and X-rays are conventional methods of diagnosing cancer, as well as endoscopy. When a tumour is recognized, a solid biopsy taken from the tumour during a surgical procedure can yield more information about the type of cancer, which is vital for deciding the treatment methods and giving the patient an accurate prognosis. However, some of the methods used for diagnosing and analysing cancer usually pose a burden onto the patient due to their invasive and time-consuming nature. Moreover, sometimes solid biopsies are even impossible to take, because the solid tumour is difficult to reach or because the surgical procedure could be too hazardous. For these reasons, a method that requires as little discomfort to the patient as drawing a blood sample is desired for diagnostics and characterization of the type of cancer.

Recently, research started focusing on liquid biopsy as an alternative to the current invasive surgical solid biopsies. During a liquid biopsy, a blood sample is drawn from the patient. As opposed to gathering information about the primary tumour retrieved from solid biopsy, the liquid biopsy is better suited to acquire knowledge about the stage of metastasis and the (biological) characteristics of the CTCs. By isolating CTCs from blood and enumerating them, the prognosis of a patient can be determined with reasonable accuracy, as a high CTC count in blood corresponds to further progressed stages of cancer and thus poorer patient survival [Qian et al., 2018].

Even though it is less physically intensive on the patient and yet at the same time more time- and cost-efficient, liquid biopsy has the potential to yield more relevant information about the most lethal aspect of the disease than its solid counterpart if viable CTCs could be succesfully isolated for further culture and analysis. If such a method could be clinically established, this could lead to significantly better personalized cancer treatment [den Toonder, 2011], as different cancers and patients need

different types of treatment.

Since microfluidics are the technologies used for precise and careful manipulation of small volumes of fluids, this field of expertise has found several ways for separating small cells and particles from fluids, including blood. As such, using microfluidics to isolate CTCs from samples might not just be useful, but even necessary to establish the desired devices. Microfluidic approaches also provide huge opportunities for culturing CTCs as they allow precise manipulation of cells in soft and three-dimensional environments as opposed to the rigid environment provided by petri dishes [Weigelt et al., 2014].

The big challenge that currently limits the development of a device capable of isolating viable CTCs lie in the scarceness of CTCs compared to the other contents found in blood. Moreover, the separation process should happen while keeping the CTCs alive. CTCs in cancer patients usually only make up 1 to 10 cells for every mL of blood, whereas the same amount of blood contains millions of white blood cells and a billion red blood cells. Besides, CTCs are shown to be quite delicate and vulnerable, especially since their unnatural occurrence in blood is often detected and taken care of by the immune system. This means that keeping this small proportion of CTCs viable for further microfluidic culture is especially challenging as well.

1.1 Goal

This research is part of an ongoing project at Eindhoven University of Technology's Microsystems group, which aims to establish a microfluidic system capable of isolating, encapsulating and culturing of circulating tumour cells. This graduation project mainly focuses on the isolation and encapsulation aspects. Circulating tumour cells are to be isolated based on protein expressions by employing magnetic particles functionalized with the specific antibody anti-EpCAM (epthelial cell adhesion molecule), which are also used in the commercial CTC-counting system "CellSearch" [Menarini Silicon Biosystems,]. As a result, a microfluidic chip with removable magnetic platform capable of capture and release of epithelial cells, i.e. EpCAM+ cells was established over the course of this project. The chip was tested with MCF-7 cell line cells, which are known to express EpCAM. Moreover, this project also explores droplet generation and encapsulation statistics of cell-like particles. The encapsulation statistics are to be used for magnetophoretic separation tests of encapsulated magnetic microparticles before testing on actual magnetically labelled cells. In the end, industrial solutions and suggestions for further research will be discussed.

2 Background and theory

2.1 Isolating CTCs

The following paragraphs detail some of the existing methods for isolating CTCs and cell-line tumour cells. These form only a small selection of the methods researched and tested for the isolation of rare cells. For a more complete overview, Appendix Table A.1 can be consulted [Ferreira et al., 2016].

2.1.1 CellSearch method

The CellSearch methodology isolates CTCs from the cells normally present in the blood (in particular white blood cells, WBCs) by employing magnetic nanoparticles functionalized with EpCAM (epithelial cell adhesion molecule) antibodies. This process starts with a 7.5 mL blood sample drawn from a patient. The CTCs (mostly of lung, breast, colorectal or prostate origin) that are inside the blood samples often express EpCAM on their membrane, whereas this expression is not as strong or even absent in normal blood cells. To make good use of this property, anti-EpCAM ferrofluid is mixed with the blood sample, where anti-EpCAM nanoparticles bind to the EpCAM on the cell membranes, allowing magnetic fields to selectively manipulate the CTCs. Next, the isolated cells are stained with fluorescent nucleic acid dye (DAPI) and labeled with antibodies to cytokeratins 8, 18 and/or 19 (anti-CK-PE) and an antibody specific for leukocytes (anti-CD45-APC). The magnetic field is applied by the MAGNEST cartridge holder. The cells that express EpCAM are magnetically attracted towards the top of the cartridge where they are imaged. CellSearch software then shows images of the cells to an operator who then manually counts and selects the cells that show all the correct markers that identify a CTC. Usually a CellSearch assay showing $>$5 CTCs in the sample implies a bad prognosis, whereas for $<$5 CTCs the prognosis is relatively optimistic. CellSearch however is not a perfect method for merely isolating CTCs, as around 1000 to 5000 WBCs with a certain degree of EpCAM expression are isolated along with the CTCs as well. Another drawback of using EpCAM to isolate CTCs is the bias towards EpCAM-positive CTCs, whereas EpCAM-negative CTCs are being left undetected, possibly leading to false negatives.

2.1.2 Other methods of isolation

A microfluidic method of isolating CTCs based on EpCAM expression is by staining the CTCs with the same or similar immunomagnetic particles as in the CellSearch procedure. The CTCs can be isolated from the other cells by active electromagnetic actuation [Jack et al., 2017]. Here, the CTCs are pulled towards one side of the channel, which at the end splits into two outlets; one for waste material and one for the CTCs. Very similarly, a method using an electrically actuated magnet (instead of a permanent one) with two FeNi wires inside the channel yielded promising results in the isolation of magnetically labeled cells [Zhi et al., 2019]. This work demonstrated that the magnetic particles laterally followed the FeNi wires to the electromagnet's side of the channel, as shown schematically in Figure 2.1:

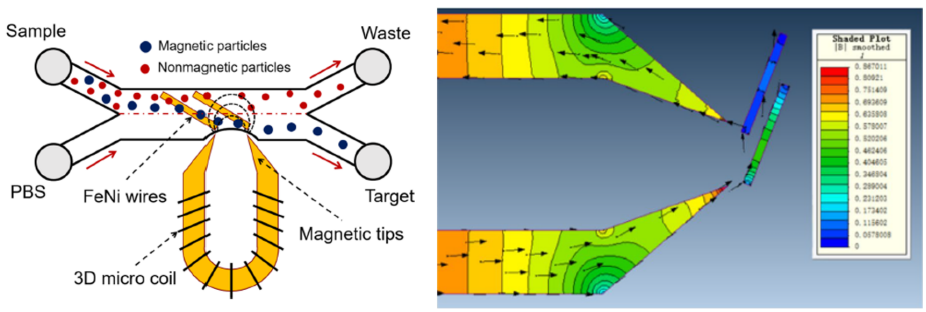

Figure 2.1: *Schematic set-up of electromagnetic isolation (left) and the magnetic flux density through the electromagnet and FeNi wires (right) [Zhi et al., 2019].*

The effectiveness of this method is established by the relatively large gradient of the magnetic flux density $\vec{B}$ as the magnetic force $\vec{F_m}$ is dependent on this gradient according to the following equation:

$$\vec{F_m} = \frac{V_b \cdot \Delta\chi}{\mu_0}(\vec{B} \cdot \nabla)\vec{B} = \frac{V_b \cdot \Delta\chi}{2\mu_0}\nabla\vec{B}^2 \tag{2.1}$$

Here V_b is the magnetic volume of the magnetic particle, μ_0 is the magnetic permeability in vacuum ($=4 \cdot \pi \cdot 10^{-7}$ H/m) and $\Delta\chi$ is the difference in magnetic susceptibility between the magnetic particle and the surrounding fluid matrix.

EpCAM+ cell-lines have also been demonstrated to be isolatable by making the medium containing the cells flow through a wide chamber with an array of permanent magnets underneath [Hoshino et al., 2011]. The combined width and height of the chamber make for relatively low velocities at reasonable flowrates to ensure sufficiently high throughput for the designated clinical use. The labelled cells were attracted to the bottom of the chip and got stuck there, after which the top part of the device could be removed to examine the cells. This chip is shown for reference in Figure 2.2:

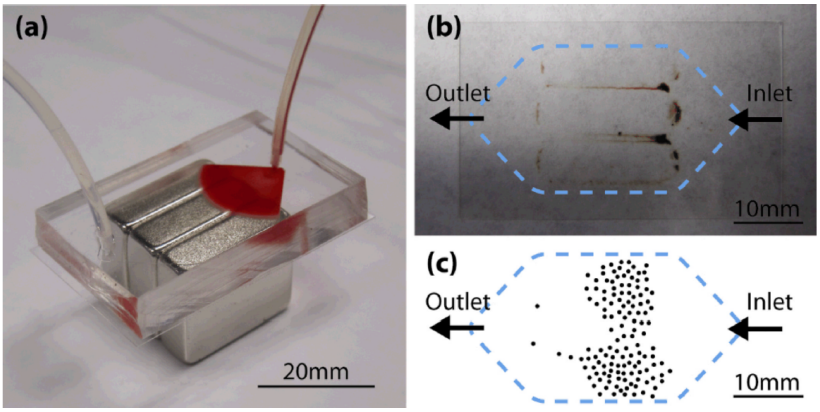

Figure 2.2: *Permanent magnet-based cell isolation chip [Hoshino et al., 2011].*

Another method of isolation by using EpCAM is by making the CTCs bind to EpCAM-antibody coated micropillars [Nagrath et al., 2007]. Although, the extra steps required to release the CTCs from the micropillars are undesirable for the intended end-product meant for clinical use.

CTCs have also shown to be isolatable by size. This can for instance be achieved by employing arrays of 'baskets' consisting of three micropillars. Due to their relatively large size and their mechanical properties -CTCs are gerenally stiffer than WBCs- CTCs get stuck in-between the micropillars, whereas regular blood cells flow right past them [Chen et al., 2017]. By reversing the direction of the flow, the captured CTCs flow out and past the micropillar 'baskets' and can be collected subsequently.

Isolation based on size by employing micropillars, however, has a drawback of exerting relatively high direct contact pressures and shear stresses on the captured CTCs. There is, however, a microfluidic method that can be used to isolate cells by size without hard contact, but by making use of flow characteristics. Particles that differ in size are exposed to drag forces and lift forces which scale differently, leading to particles of certain sizes going to a specific position along the width of the channel, leading to isolation by flow dynamics. A narrow-channel spiraling flow generates a secondary flow perpendicular to the general flow direction. This secondary flow consists of two vortices, rotating as demonstrated in Figure 2.3 [Al-Halhouli et al., 2018]. This secondary flow type is called a Dean flow. The similarities in dimensions between WBCs and CTCs, however, make it difficult to isolate these two types of cells with this principle.

Inside a Dean flow, the larger particles experience relatively strong lift forces, whereas the smaller particles experience a relatively high flow friction force. As a result, the Dean flow pulls the smaller

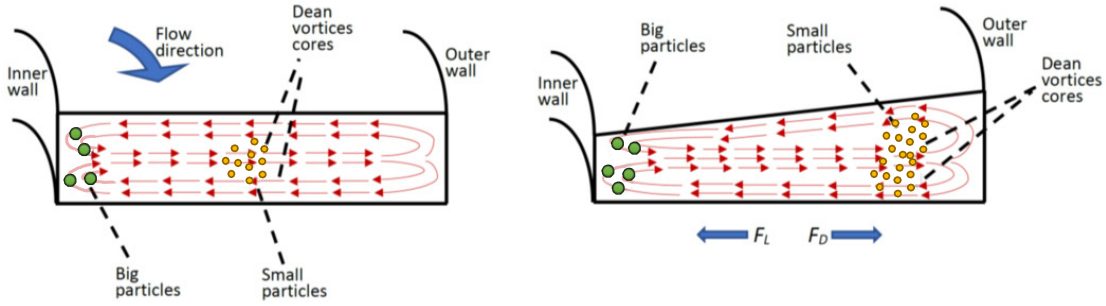

Figure 2.3: *Isolation of particles based on size. Adapted image adapted from [Al-Halhouli et al., 2018].*

particles towards the outer wall of the curvature while the larger ones mostly remain close to the inner wall. For CTCs in blood, this method can be used to isolate larger cells from the red blood cells, however, since WBCs and CTCs are similar in size, this method is less suited for the isolation of these types of cells.

2.1.3 Resulting velocity due to actuation forces

In microfluidics, the small size of particles in the flow causes body forces on particles to be negligible compared to the drag forces. This means that when such a force is being applied on a small particle (for instance gravitationally, magnetically or electrostatically) in a microfluidic channel, the action force is almost immediately counteracted by a resulting drag force. As a result of force balance and negligible inertia, the relative velocity caused by this force is quite well defined. For a spherical particle, the drag force due to flow velocity can be calculated by equating the magnetic action force to Stoke's drag force Equation 2.2 and rewriting for the velocity 2.3:

$$F_{act} = -F_{drag} = 6\pi r\eta v \tag{2.2}$$

$$v = \frac{F_{act}}{6\pi r\eta} \tag{2.3}$$

In these equations, F is the force, η is the dynamic viscosity, v is the flow velocity difference between particle and fluid and r is the radius of the spherical particle. Since this research focuses on CTC isolation through magnetics, the magnetic force on small particles should be known in order to estimate the settling time of magnetically labelled cells. For small particles inside a magnetic field, the force can be calculated as stated in Equation 2.1. By combining Equations 2.1 and 2.3, Equation 2.4 can be constructed and the order of magnitude of the settling velocity of small magnetized particles can be calculated when all parameters are known:

$$v = \frac{\Delta\chi V \nabla \vec{B}_y^2}{12\mu_0 \pi \eta R} \tag{2.4}$$

2.1.4 Quantification of isolation

There are several ways to determine the effectiveness of CTC isolation [Ferreira et al., 2016]. These methods, although similar, clarify different aspects of the capture processes. To test the quality of isolation for a certain method, usually controlled amounts of cells from cultured cancer cell lines are used. This known amount is then compared to the actual amount of isolated cells. However, tumour cells from cell culture lines are more distinct from leukocytes than CTCs. This possibly leads to over-estimating the device performance when testing with samples that have been spiked with cell line tumour cells. The following part details some of the methods used to quantify the quality of isolation, when using these well-controlled samples.

The capture efficiency is the simplest way of characterizing the performance and is defined as the ratio between captured CTCs and actual amount of CTCs. Ideally, its value should approach 1:

$$CaptureEfficiency = \frac{TCs_{captured}}{TCs_{actual}} \tag{2.5}$$

Enrichment is similar to, yet different from capture efficiency as it takes the capture of unwanted captured $WBC_{captured}$ and initial amount WBC_{in} of white blood cells into account as well. Enrichment is the ratio of the proportion CTCs to WBCs after and before CTC isolation. Optimally, its value should approach infinity as the ideal amount of captured WBCs is zero.

$$Enrichment = \frac{TCs_{captured}/WBCs_{captured}}{TCs_{actual}/WBCs_{in}} \tag{2.6}$$

Then, there is purity, which is the relative amount of relevant cells compared to the total amount of captured cells (CTCs and WBCs). As the amount of WBCs captured should be as low as possible, the value of purity ideally is equal to 1:

$$Purity = \frac{TC_{capt}}{(TCs + WBCs)_{capt}} \tag{2.7}$$

And finally viability, the amount of cells alive after enrichment relative to the total amount of cells.

2.2 Bead formation techniques

In order to make a CTC culture that resembles the in vivo situation, in this case of breast cancer, the basement membrane around the tumour can be modelled by encapsulating tumour cells in gel beads, e.g. Matrigel. The stromal extracellular matrix can be modelled by embedding these beads into collagen-I [Jelle J. F. Sleeboom, 2018]. Figure 2.4 shows the similarities and differences between a healthy mammary gland, cancer growth in vivo and a microfluidic model established to replicate cancer growth.

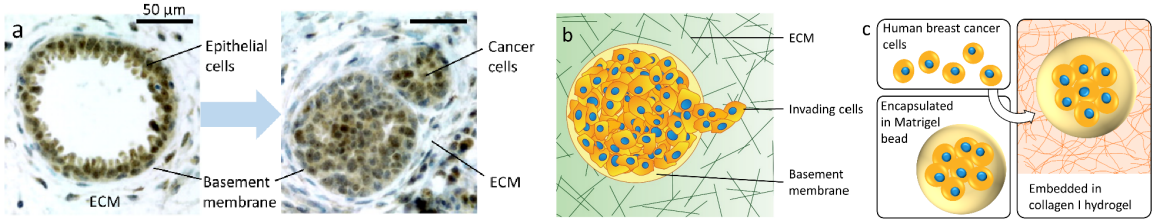

Figure 2.4: *Similarities between the breast cancer tumour microenvironment and the model: a) healthy and tumour breast tissue, b) schematic of tumour growth and invasion, c) schematic of the model established by microfluidics. Adapted from [Jelle J. F. Sleeboom, 2018].*

Several microfluidic techniques exist to create droplets in oil. Microfluidic beads can be made by first making droplets, followed by a method to either solidify or gelate these droplets. Creating the desired interface requires at least two separate phases, coming from separate inlets; one for the droplet aqueous phase (also known as the dispersed phase) and one for the continuous (or matrix) oily phase. More complex beads (>2 phases, e.g. water-in-oil-in-water-in-oil) can also be created with additional inlets [Shah et al., 2008]. A method where the bead-in-oil interface is created by a nozzle inside another channel is called the co-flow principle, illustrated in Figure 2.5.

Figure 2.5 shows that droplets can be formed in two regimes of flow; either by dripping (a, b) or by jetting (c). These two regimes are dependent on two characteristic dimensionless numbers, the inner Weber number and the outer capillary number. These numbers are defined as follows:

$$We_{in} = \frac{\rho_{in} d_{tip} u_{in}^2}{\gamma} \tag{2.8}$$

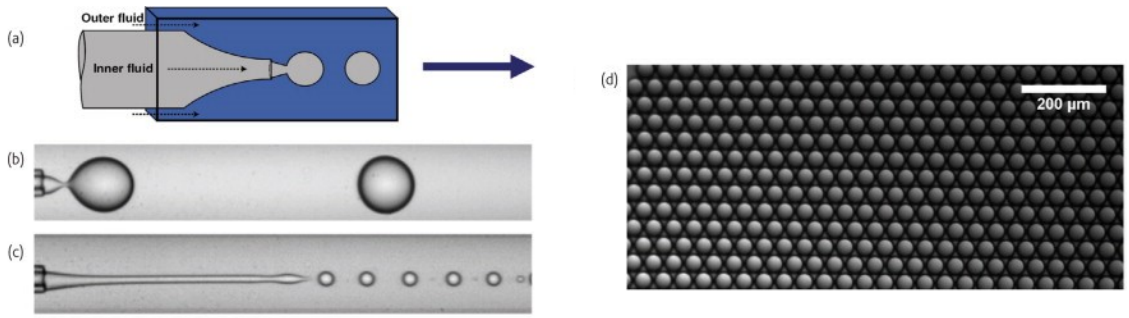

Figure 2.5: *Co-flow microcapillary device [Shah et al., 2008]: a) schematic overview, b) dripping regime and c) jetting regime of droplet generation, d) generated droplets.*

$$Ca_{out} = \frac{\eta_{out} u_{out}}{\gamma} \tag{2.9}$$

Here, ρ is the density of the dispersed (droplet) phase, d_{tip} is the diameter of the nozzle where the droplet phase enters the continuous phase, u_{in} is the mean velocity of the droplet phase and u_{out} is the mean velocity of the continuous phase, η_{out} is viscosity of the continuous phase and finally γ is the surface tension between the two phases. Dripping occurs when both capillary number and Weber number are low as demonstrated in Figure 2.6 [Utada et al., 2007]:

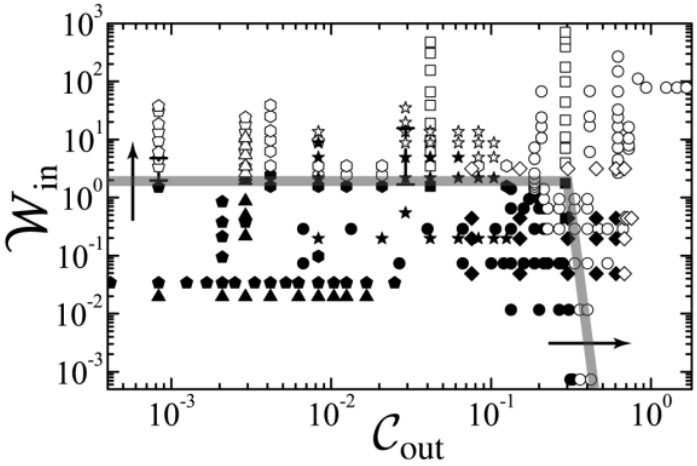

Figure 2.6: *Jetting and dripping regimes; filled symbols represent dripping whereas open symbols represent jetting.*

The flow-focusing principle is similar to, yet completely different from the co-flow principle. Here, by using both sides of the outer channel as inlets, the inner channel consequently becomes the outlet where droplets or beads can be formed, as demonstrated in Figure 2.7.

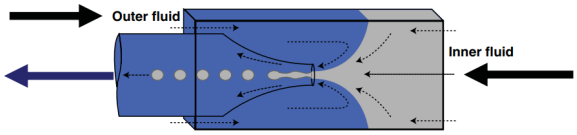

Figure 2.7: *Flow-focusing microcapillary device [Utada et al., 2007].*

Unfortunately, it is not quite straightforward to manufacture a channel inside another channel at these small scales of microfabrication. There is however a in-plane solution to make beads in oil,

which has already been demonstrated to work for encapsulating MCF-7 cell line tumour cells in Matrigel beads [Jelle J. F. Sleeboom, 2018]. This work demonstrated a channel structure similar to the schematic shown in Figure 2.8, where inlet A provided the continuous oil phase and inlet B provided the dispersed phase of MCF-7 cells suspended in Matrigel. Due to the oil coming from the sides of the Matrigel-MCF-7 supply and the resulting surface tension, the Matrigel flow broke up into droplets containing MCF-7 cells at the intersection where the flows merged.

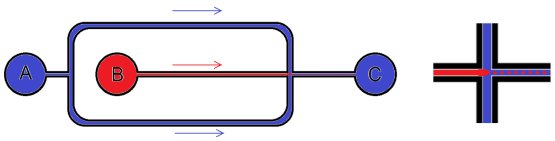

Figure 2.8: *Schematic 2D flow-focusing principle.*

Since this is a simple channel structure, this design can be fabricated by following straightforward lithography steps while using PDMS as base material. The part detailed in the schematic in Figure 2.8 was only half of the chip. Since the droplets needed to gelate after formation in a controlled fashion, a second part was needed. Matrigel, which was used as the droplet phase in Sleeboom's work, is liquid when kept under cool conditions and gelates at elevated temperatures. As such, the droplet formation part was to be kept relatively cool to keep the Matrigel liquid during droplet formation. The second half of the chip's structure consists of a relatively warm meandering channel. The elevated temperature in this channel and its length are necessary to provide the required heat and time to induce gelation of the MCF-7 in Matrigel droplets after formation, as demonstrated in Figure 2.9.

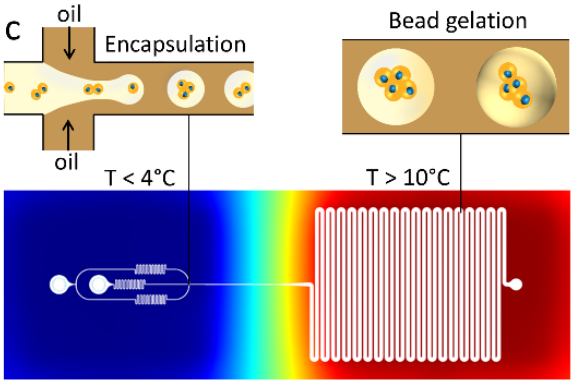

Figure 2.9: *Encapsulation and gelation of CTCs in Matrigel [Jelle J. F. Sleeboom, 2018].*

The local temperatures in this chip were controlled by heat transported in water underneath the chip through a chip-holder. The chip-holder was constructed with laser-cut elements that made the fluid compartments for either cooling or heating align with the design of the microfluidic droplet generator. A compartment of air was included in-between the heating and cooling compartments as isolation. Proper thermal contact was established by introducing a wetting layer of water in-between the microfluidic chip.

Droplet microfluidics have been used to encapsulate cells and particles for a multitude of purposes. In this research, the purpose is to create controlled, reproducible environments in which CTCs can proliferate. A fundamental principle that prevents total reproducibility is the Poisson distribution. The Poisson distribution is a discrete probability distribution that can be used to describe the amount of events occurring in a certain amount of time. Many Poisson-distributed phenomena can be observed in nature. In droplet microfluidics, the Poisson distribution can be used to describe and predict the amount of particles passing the droplet formation nozzle during the formation of a single droplet. Consequently it dictates the random distribution of particles inside a droplet for a certain mean number of droplets. The mean number of particles per droplet can be tuned by varying the

concentration of suspended cells or particles inside the dispersed phase and by tuning the continuous phase flowrate to adjust the size of the droplet which contains these particles and cells. The Poisson distribution is characterized by its variance (λ) being equal to its mean (λ). The probability density function is governed by Equation 2.10:

$$P(X = k) = \frac{\lambda^k}{k!} e^{-\lambda} \tag{2.10}$$

Here, P is the possibility of counting a total of k particles inside a droplet for a population average of λ. The distribution is positively skewed for relatively low values of λ and it becomes more symmetric for increasing λ, as it approaches a discrete normal distribution. Examples for the Poisson probability density function for several values of λ can be found in Figure 2.10:

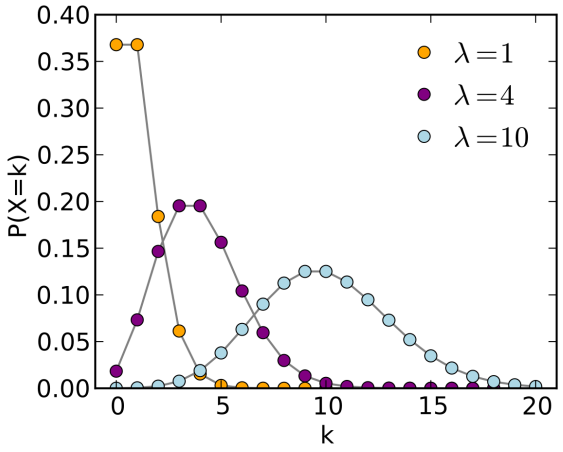

Figure 2.10: *Poisson distriubution for various* λ.

The mean number of particles or cells per droplet can be determined by first calculating the volume of the desired droplets and determining the desired average λ. The amount of particles per droplet can be converted to the desired concentration via Equation 2.11:

$$C = \frac{\lambda}{V} = \frac{4\lambda}{3\pi r^3} \tag{2.11}$$

Here C is the suspension concentration, λ is the desired average amount of particles in a droplet, V is the volume of the droplet and r is the radius of the droplet, assuming spherical droplets). If encapsulation of multiple particles or cells in one bead is undesirable, λ should be tuned such that the probability of having 2 or more particles in a droplet approaches zero, and all droplets either contain 1 or no droplets.

3 Magnetic isolation

One of the goals of this project was to design a device for the magnetic isolation of EpCAM+ cells and EpCAM+ cell-containing droplets from their non-labelled counterparts. In order to achieve this, an initial exploration of the properties of cubic magnets was done to establish a decent understanding of the physics behind magnetism. This knowledge was then used for the implementation of magnets into the designed isolation devices. The following sections will discuss the numerical and experimental exploration of magnetic properties of cubic magnets, followed by on-chip cell capture by use of magnetic platform. In the end, attempts for making a continuous flow isolation device will be discussed.

3.1 Computational analysis

Permanent magnets are extraordinary, versatile and sometimes quite unpredictable blocks of metal that can attract and repel other magnets with varying force. This phenomenon mostly depends on orientation, distance, size and material properties. Arrays of magnets are also able to strengthen and weaken the magnetic fields compared to single magnets based on the same dependencies. The computational and experimental exploration of linear and planar arrays of magnets will be discussed in the following paragraphs.

Generally speaking, magnets are too complex for simple calculations. Especially in the case of magnet arrays and for the interactions between magnetic elements, the use of finite element method (FEM) approaches is necessary to utilize and and explain the magnetic behaviour. In the following paragraphs, a summary of the performed magnetic simulations will be given. The main idea is that for any small magnetic micro-/nanoparticle in a magnetic field, Equation 2.1 is valid to calculate the resulting magnetic force. To recapitulate, this equation was:

$$\vec{F_m} = \frac{V_b \cdot \Delta\chi}{\mu_0}(\vec{B} \cdot \nabla)\vec{B} = \frac{V_b \cdot \Delta\chi}{2\mu_0}\nabla\vec{B}^2 \tag{3.1}$$

Since the main goal was to model and optimize the magnet array for magnetic force, the main point of interest was to maximize $\nabla\vec{B}^2$ as the magnetic volume and magnetic susceptibility are constants for a given type of small magnetic particle. For this reason, the following paragraphs will focus on calculations of $\nabla\vec{B}^2$ since this parameter is proportional to the magnetic force on a particle that can be tuned and optimized by varying system dimensions.

3.1.1 Linear arrays

Initially, the main plan was to optimize the effectiveness of the available magnets by organizing them in smart configurations, starting with linear arrays of cubic magnets. A famous array type to strengthen the magnetic field is the Halbach array. By rotating each following magnet's polarity by 90 degrees, one can create a magnet array with a relatively strong side and a relatively weak side. A visualization of such an array is given in Figure 3.1a. Another method to strengthen magnets is by swapping the polarity by 180 degrees for each following magnet in the array as demonstrated in Figure 3.1b:

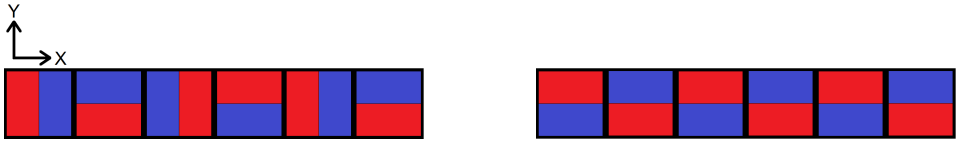

(a) *Halbach array, strong side up.* **(b)** *Swapped polarity.*

Figure 3.1: *Schematic of the two types of linear magnet configurations as analysed in COMSOL Multiphysics. Red represents the magnetic north. Blue the magnetic south pole.*

The swapping polarity has the benefit of not requiring any glue or mechanical support to keep the magnets in a straight array. In practice, the Halbach array required a slot where it would be kept in place as demonstrated in Appendix Figure A.1. To model the magnetic field strength of these arrays, a 2D FEM analysis was done in COMSOL Multiphyisics for infinitely long magnet arrays by using periodic boundary conditions around four cubic magnets with dimensions of 5 mm (lenght, width and height). The remanent magnetization of each individual magnet was normalized to 1.00 T, which is a decent estimate for the magnetization of the acquired neodymium magnets that were used over the course of this research. Three plots were made for every situation, with directions referring to the directions shown in Figure 3.1a:

a. A 3D surface plot was made for the magnitude of $\nabla \vec{B}_y^2$ with respect to the parallel position to the array (x) and the perpendicular distance to the magnet array (y).

b. The magnitude of $\nabla \vec{B}_y^2$ was calculated in the field x,y-field above the magnet array and for each situation a plot was made with the values of $\nabla \vec{B}_y^2$ with respect to the x-coordinate at constant values of y. Each curve from top (blue) to bottom (orange, yellow, ...) represents a distance to the magnets of 0.5, 1.0, 1.5, ... mm, respectively.

c. A plot was made of the averaged values of the magnitude of $\nabla \vec{B}_y^2$ along the magnetic array, with respect to y. The errorbars show one standard deviation, since the value for $\nabla \vec{B}_y^2$ was not constant at every equidistant point above the array, as plotted in (b). As a result here too, each datapoint represents a distance from the magnets starting at 0.5 mm with a 0.5 mm step size.

First, evaluations were made for the strong and weak side of the Halbach array. The results are displayed in Figure 3.2 and 3.3 respectively.

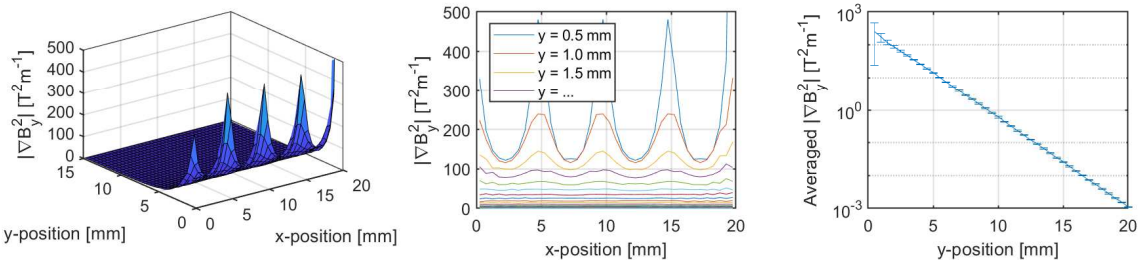

Figure 3.2: *Values of $\nabla \vec{B}^2$ for the strong side (top) of the 2D modelled Halbach array from Figure 3.1a.*

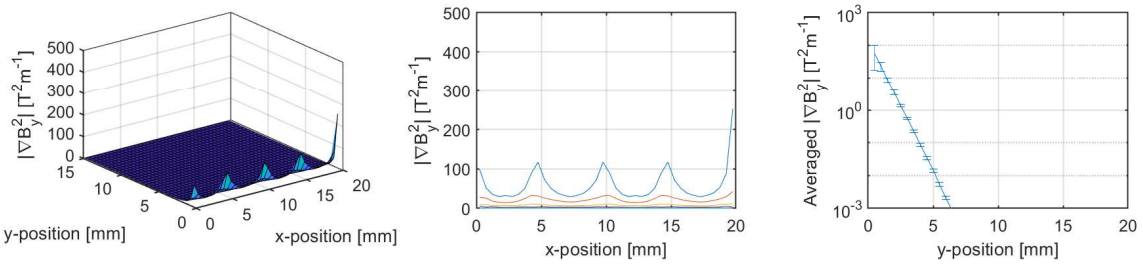

Figure 3.3: *Values of $\nabla \vec{B}^2$ for the weak side (bottom) of the 2D modelled Halbach array from Figure 3.1a.*

To compare the value of $\nabla \vec{B}^2$ with a more stable configuration of magnets, the array of Figure 3.1b was also modelled with four magnets.

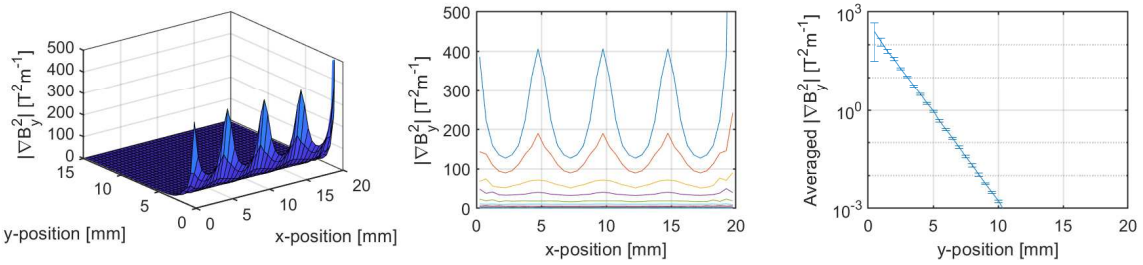

Figure 3.4: *Values of $\nabla \vec{B}^2$ for the 2D 180^o swapped polarity configuration from Figure 3.1b.*

As there is a lot of data to be found in these figures, the data should be simplified. The fact that the third figure shows a nicely declining exponential relation between $\nabla \vec{B}^2$ means that an exponential fit can be found along the datapoints. The fitting parameters of the fitting Equation 3.2 are given in Table 3.1 for this specific system:

$$\vec{F}_{magn,y} \sim \nabla \vec{B}^2 = a \exp(-b \cdot y) \tag{3.2}$$

Table 3.1: *Fitting parameters for the simulation results for different magnet configurations.*

Configuration type	a	b
Halbach strong side	3.2e2	0.62
Halbach weak side	1.6e2	1.89
Switching polarity	4.6e2	1.26

From the plots made in Figures 3.2, 3.3 and 3.4 and the fits, it can be concluded that the order of magnitude of $\nabla \vec{B}^2$ for both the strong side of the Halbach array and the swapping polarity array is around 300 to 400 close to the magnet array. For increasing distance however, this value seems to drop significantly slower for the stronger side of the Halbach array compared to the swapped polarity configuration.

3.1.2 Planar arrays

In order to allow high flowrates while ensuring sufficient residence time in the presence of the magnetic field, microfluidic channels can be widened and deepened. However, the magnetic force on small particles decreases exponentially with increasing distance from the magnet arrays, as shown in the previous section. This is undesirable for the magnetic isolation mechanism. As a consequence, plans were made to apply magnetic arrays to the bottom of a wide channel. With this method, the channel could almost be made as wide as possible without the hazard of decreasing the minimum magnetic field strength at the furthest parts from the magnetic array since channel height would not be affected. The types of planar magnet arrays we considered are displayed in Figure 3.5.

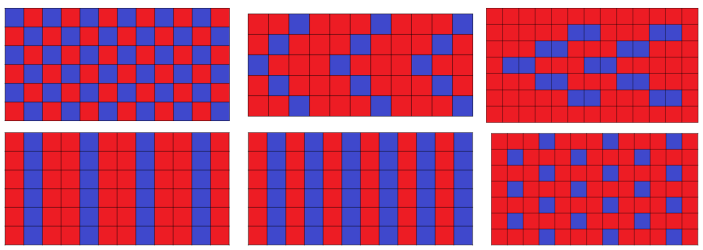

Figure 3.5: *Several cube magnet array types designed to be underneath the isolation device flow channel; flow direction from left to right. Red represents the magnetic north. Blue the magnetic south pole.*

Attempts to fabricate stable versions of these srray designs were done before further analysis. Only the top-left checkerboard-like magnetic array configuration appeared to be stable without the use

of external factors like glue. As such, this type of array was chosen for further evaluation. For this type of planar array it was noticed by practical observation that the elevation above the magnet arrays dictates where the magnetic micro particles were most likely to migrate towards in case of a checkerboard-like magnet array. For a small distance up until approximately 300 µm the particles would migrate towards the edges of the magnets, whereas at approximately over 700 µm above the magnets the particle would migrate towards the center of the magnets as demonstrated in Figure 3.6. In-between these distances there is a transition taking place.

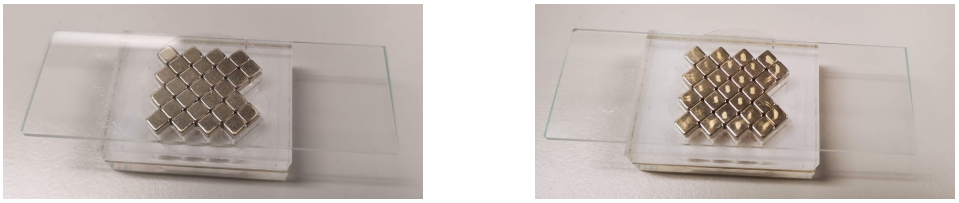

(a) *distance = 0.1 mm, coverslip facing down.* **(b)** *distance = 1.0 mm, microslide facing down.*

Figure 3.6: *Micromod's micromer 10 µm magnetic microparticles suspended in water in-between a microslide and a coverslip, agglomeration (beige) due to magnetic interaction.*

Initially the expectation was that the magnetic particles would migrate towards the edges of the magnets in the planar array. To explain the observed behaviour a 3D simulation was executed to capture what was happening in this case. Arrays of four cubic magnet halves were analysed with periodic boundary conditions in the planar (x,y) directions. Antisymmetry conditions were used in the perpendicular (z) direction to model only the magnetic north. Again, the remanent magnetization of each magnet was normalized to 1. The mesh-size was set to 'extremely fine', which is the most detailed mesh option. A front view of a 2D slice showing the values of $\nabla \vec{B}_x^2$ on a color scale shows that the directionality of the in-plane components of $\vec{B}^2$ indeed swaps at a certain elevation above the magnet surface. This can either be observed by looking at the colors red and blue swapping and by the normalized arrows displaying the direction of $\nabla \vec{B}_x^2$ shown in Figure 3.7:

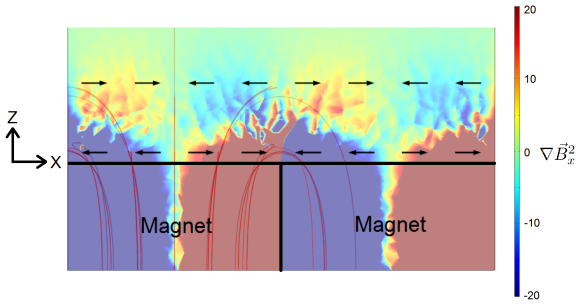

Figure 3.7: *Direction of the in-plane x-component of $\nabla \vec{B}_x^2$ indicated by colors and arrows, slice going through the center of a 4 mm cubic magnet.*

In order to map the direction of the force in the 2-dimensional plane above the magnet surface, animations have been made that show the direction of the in-plane forces with arrowheads. The magnitude of the force is given by a color scale. Links to these animations are given in Appendix A.3. Images were taken to visualize the in-plane direction of the magnetic force on the microparticles in still images by using the same model. These images are shown in Figure 3.8 below:

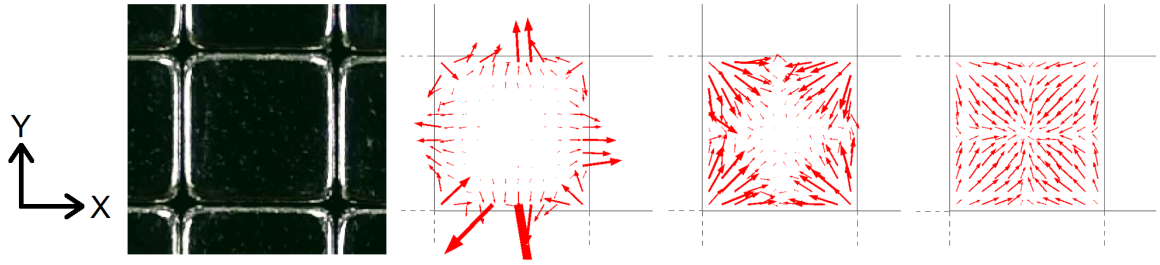

Figure 3.8: *Arrow surface of $\nabla \vec{B}^2_{x,y}$ at 0.2, 0.7 and 2 mm above the magnet array, not to scale in-between images. Photo on the left is a visualization of the simulation location with regard to the actual magnets. Dashed lines represent magnets that were omitted in the simulations through the use of periodic boundary conditions.*

These images also show that there is indeed a certain elevation above the magnets where the location where the direction of transport of the magnetic particles changes. Note that there are some outlier arrows at the bottom of the leftmost image in Figure 3.8. This is most likely a computational error of which the cause is unclear. This COMSOL model was also used to analyse perpendicular forces. By equally spacing 21 slices above the magnet arrays, ranging from 0 to 10 mm, the global average and standard deviation of the magnitude of $\nabla \vec{B}^2_z$ were calculated for each slice. The model contained 20 mm of space in z-direction above the magnet array to minimize the influence of boundary effects. This analysis was repeated for cubic magnets of 1, 2, 4, 8 and 16 mm. The results can be found in Figure 3.9:

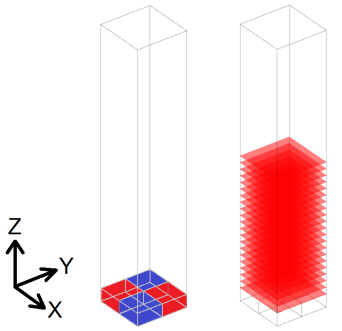

(a) *Schematic of 4 magnet halves (left), including 21 slices for analysis (right).*

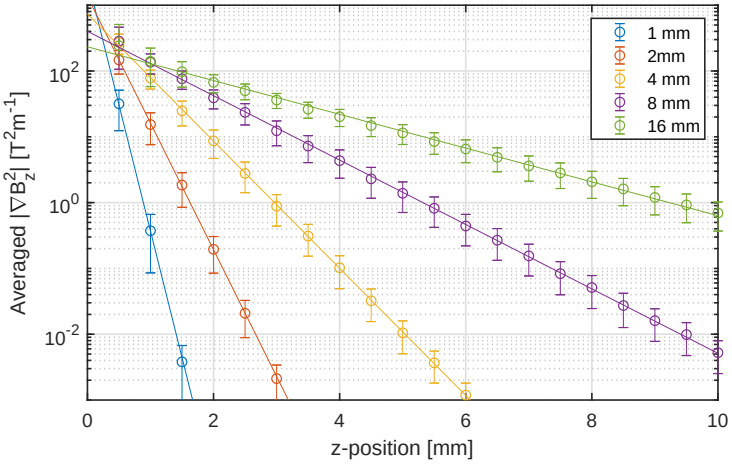

(b) *Magnitude of $\nabla \vec{B}^2_z$ for increasing z and various magnet sizes.*

Figure 3.9: *COMSOL evaluation of $\nabla \vec{B}^2$; schematic of the periodic system and corresponding results.*

The 3D situation for arrays of all magnet sizes also showed a good correspondence to Equation 3.2. As such, the fitting parameters could also be computed for the three-dimensional situation. Convergence of $\nabla \vec{B}^2_x$ of all curves can also be observed by eye for z approaching zero. A further zoom-in display of the upper left part of Figure 3.9b can be found in Appendix Figure A.4. In order to analyze this further, the fitting parameters were put in Table 3.2:

Table 3.2: *Fitting parameters of the curves shown in Figure 3.9b.*

d_{magnet}	a ($\cdot 10^3$)	b
1	2.54	8.83
2	1.36	4.43
4	0.73	2.22
8	0.40	1.13
16	0.23	0.59

These fitting parameters followed a well-defined pattern as well, as they showed strong linearity in a double logarithmic plot, as displayed in Figure 3.10:

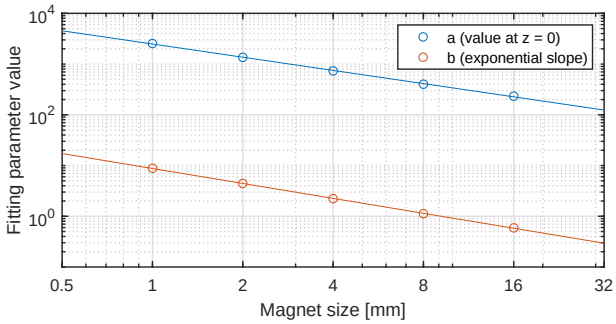

Figure 3.10: *Fitting parameters of a and b from Equation 3.2 for the curves shown in Figure 3.9b.*

These well-defined fitting parameter characteristics could allow optimization for choosing the magnet sizes used in the arrays, depending on the shortest magnet-to-channel distance achievable.

Since the order of magnitude of $\vec{B}_z^2$ is now known, this value can be used to estimate the resulting vertical velocity which is necessary to estimate the required residence time in the magnetic chamber for a magnetic particle to settle. To do this, Equation 2.4 is recapitulated:

$$v_z = \frac{\Delta\chi V \nabla \vec{B}_z^2}{12\mu_0 \pi \eta R} \tag{3.3}$$

By making educated assumptions for the values of the parameters in this equation, a typical particle velocity v_z can be calculated. Estimations for these parameters can be found in Table 3.3.

Table 3.3: *Estimated parameters for Equation 2.4.*

Variable	Symbol	Value	Unit
Dynamic viscosity	η	0.1	Pas
Radius of cell	R	5e-6	m
Out of plane gradient of B^2	$\nabla \vec{B}_z^2$	100	T^2/m
Magnetic susceptibility	$\Delta\chi$	10	-
Magnetic volume (1% of V_{cell})	V	5.24e-18	m^3
Magnetic permeability	μ_0	1.257e-6	H/m

By using Equation 3.3 and the values in Table 3.3, a settling velocity of approximately 0.2 mm/s was found for a magnetically labelled cell located 1 mm away from a magnetic array at most.

3.2 Device design and fabrication

A microfluidic cell isolation chip along with a corresponding magnetic platform have been designed to allow the capture and release of EpCAM+ cells with CellSearch's anti-EpCAM ferrofluid and capture enhancer. This section discusses the design process, assembly and results regarding this device.

3.2.1 Goal

In order to establish CTC cultures with microfluidic technologies, the first step would be to enrich and purify the CTC sample as collected from the patient. Moreover, the desired device should be able to process a patient sample ($\pm$ 7.5 mL) in matters of minutes to maybe a couple of hours. This implies that the device that is to be established should be able to process relatively high flowrates in comparison to regular microfluidic devices. As a result, the device should be able to process several millilitres per hour or preferably even process millilitres in a matter of minutes.

3.2.2 Design

First of all, the final design of the microfluidic CTC isolation device should be able to process 7.5 mL of patient sample within a reasonable time scale (in the order of an hour) whilst minimizing loss of cells and cell deaths as the cells are eventually to be embedded in collagen for cell culture. Since the CTCs that need to be isolated can best be distinguished from the other components of the sample by magnetic labelling, a magnetic approach is preferred. As stated before, cell-sorting by size would be difficult, since tumor cells are similar to leukocytes in this regard. Moreover, a simpler design is easier to mass-manufacture for disposable clinical applications. As a result it would be desirable for the design of the microfluidic components to allow mass-scale production. The magnetic actuation part does not necessarily need to be mass-producible as it can be reused after evaluating a sample as long as there is no direct contact between the sample and the actuator. However, in order to minimize the complexity of the device, permanent magnets are being preferred.

Most importantly, the cells should survive the isolation step and be recoverable afterwards for further evaluation. This means that violent (e.g. high shear) isolation approaches and permanent surface bonding approaches for isolation are not suitable for this application. In practice, only the top left (checkerboard-like) array from Figure 3.5 would be stable when the top-faces of the magnets were aligned in the same plane. In the other cases the magnets would either pop out or shift significantly. Since this shifting could cause stresses and deformations onto the bottom plate of the microfluidic cell-isolation chip, the checkerboard-like magnet configuration was chosen for this device.

The approximated settling velocity v_z of 0.2 mm/s and the desired processing time of around one hour for 7.5 mL of sample can be used to make estimations for designing a magnetic cell isolation chip. Channel height (h_c) was planned to be 200 µm at most to maintain a strong magnetic field throughout the whole domain of the channel. This implied that magnetically labelled cells should have a transition time through the magnetic domain of at least 1.0 second to properly settle towards the bottom of the chip. To achieve a sufficient flowrate and still maintain plenty of transition time, the width of the channel (w_c) was set at 10 mm. As a result, the designed cross-section of the channel was 2 mm^2, assuming a rectangular cross-section. The desired flowrate of approximately 7.5 mL/hr amounts to 2.1 µL/s. The flowrate (Q) and channel cross-section (A) were used to calculate the mean transition velocity through the designed channel by using Equation 3.4, which was 1 mm/s.

$$v_{tr} = \frac{Q}{A} = \frac{Q}{w_c \cdot h_c} \tag{3.4}$$

A two-dimensional schematic showing the general isolation and design principles can be found in Figure 3.11.

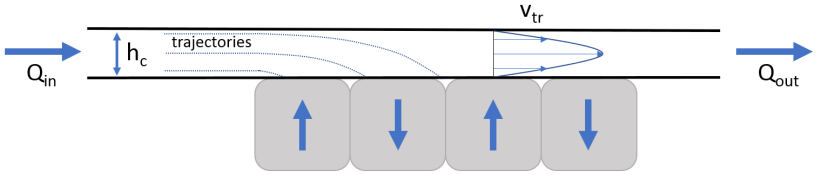

Figure 3.11: *Two-dimensional schematic of the magnetic isolation principle.*

To allow both capture and release of magnetically labelled cells, the microfluidic chip and the magnetic array should be detachable. As such, the principle shown in Figure 3.11 should not consist of a single unit, but rather two detachable ones. As a consequence, both a reusable magnetic array platform and disposable single-use chip were designed.

The chip contained a thin bottom plate with a wide channel segment (w_c = 10 mm, h_c = 0.2 mm), which spanned 20 mm. At the ends of this segment, the side-walls converged towards the inlet and outlet. The magnetic array consisted of 54 cubic magnets which were press-fitted in a custom-made slot to limit relative movement, which formed the basic principle of the magnetic platform. The magnet array inside the magnetic platform was put on a 45 degree angle to establish similar magnetic profiles along any streamline inside the chip. The chip and the platform both had outer dimensions of 40 mm x 50 mm. 3D renders of the designs can be found in Figure 3.12.

(a) *Trimetric view.* **(b)** *Top view.*

Figure 3.12: *Schematic display of the magnetic array and the isolation chamber.*

3.2.3 Fabrication

The magnetic platform mainly consisted of laser-cut PMMA with double sided tape and magnets:

a. Top section of 2 mm PMMA
b. Middle section of 6 mm PMMA sandwiched between double sided tape
c. Bottom section of 2 mm PMMA
d. 54 cubic magnets of 3.73 mm
e. A 1 mm thick PMMA insert(s)

First, the magnet array was made to fit the designated magnet slot. Attention to the desired magnet orientation was kept at all times. From experience, the alignment of magnets was easiest by first making the diagonal lines of magnets followed by assembly of these lines as displayed in Figure 3.13.

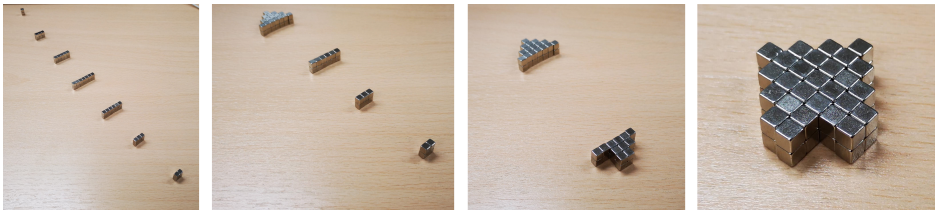

Figure 3.13: *Assembly of the magnet array.*

First, the bottom and the middle section were carefully manually aligned and fixed to each other. Inserts of 1 mm thick PMMA were used to cover the bottom of the magnet slot. Next the magnet array was inserted into the slot, resulting in magnets protruding beyond the PMMA surface. The

protruding magnets served as an alignment tool for the top section of PMMA. the top section was then carefully lowered onto the middle section and fixated. The 1 mm PMMA strips provided the right elevation to keep the top surfaces of the magnets in-plane with the PMMA platform.

The isolation chamber chip was made in a similar fashion. This chip consisted of PMMA parts and double sided tape. In order from top to bottom, the chip contained:

- A top layer of 6 mm PMMA with inlets.
- A middle layer of double sided tape, containing the channel structure.
- A bottom layer of 125 µm PMMA sheet.

Again, all parts were laser-cut. Double sided tape was cut separately with no PMMA attached by covering both sides of the tape with its proprietary protective foil. The 6 mm PMMA top layer was then carefully aligned with the tape containing the channel structure. The parts were subsequently fixed. The thin 125 µm PMMA sheet was carefully fixated to the other side of the tape after. Unwanted air inclusions in-between PMMA and tape were found to be reducible by applying gentle pressure with the thumb or index finger during fixation of the parts. The construction phases of these parts are demonstrated in Figure 3.14.

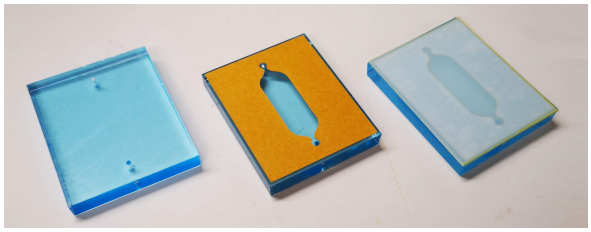

Figure 3.14: *Construction of the isolation chip. Form left to right: 6 mm PMMA top layer, double sided tape added on top, thin film PMMA added to seal the chip bottom surface.*

The inlet and outlet of the device were made by taking 20 gauge dull syringe needles (Techcon Systems, China) and removing the plastic luer-lock thread. The needle was carefully bent to approximately a 90 degree angle while preventing buckling of the needle. To make the connection between the syringe needle waterproof, 5 mm lengths of 0.034" inner diameter tubing (Scientific Commodities, U.S.A.) were cut at approximately 45 degree angles and pressed onto the needle ends that would be directly inserted into the chip. The covered needle ends were then inserted into the chip with the tubing serving as waterproof sealant. This method proved to be watertight beyond flowrates of 1 mL/min.

In order to keep the chip and magnet array fixed with relation to each other, a boundary frame with an edge thickness of 5 mm and a height of 12 mm was made to restrict relative relative planar translational motion and rotational motion of the chip and magnetic platform. The designs as shown in Figure 3.15 were used during the testing phase of this research, which will be detailed in Section 3.3.

(a) *Separate parts.* **(b)** *Assembled parts.*

Figure 3.15: *Magnetic platform, frame and the chip (including inlet and outlet needles)*

3.3 Experiment

3.3.1 Methods

Tests with the device described in the previous section were executed inside the cell laboratory at the Microsystems group of TU/e. In order to count cell concentrations, Nucleocounter NC-200 and VIA1 cassettes were used. MCF-7 cells were obtained during passaging. As suggested by our partners of Erasmus UMC, 15 microlitres of both CellSearch's EpCAM ferrofluid and capture enhancer were used inside every 1000 µL of used cell suspension to make the cells susceptible to magnetic fields. These concentrations are of the same order as the actual concentrations of ferrofluid and enhancer used in the CellSearch System as a 16-assay kit contains vials of 3 mL of these agents. This corresponds to 25 µL per mL whole blood, assuming sixteen 7.5 mL assays. The desired flowrates were applied with simple syringe pumps (PumpSystems inc. and Chemyx) with various plastic syringes mounted on top. The passaging protocol was used as provided by J.J.F. Sleeboom and can be found in Appendix A.5.1. A detailed protocol of the test will be explained below.

Two lengths of tubing were cut and connected to both syringe needles inside the isolation chamber. A 10 mL syringe was taken and pre-filled with a known volume of usually 3 to 5 mL of de-ionized water. A 1 mL syringe was used as a reservoir for the cell suspension. As such, the plunger was removed from this syringe. Both syringes were then carefully secured to the tubing on both ends of the isolation chamber chip via luer-lock syringe needles. Next, the pre-filled 10 mL syringe was used to pre-fill the whole system until the de-ionized water reached the bottom of the 1 mL syringe. Afterwards the 10 mL syringe was mounted on top of the syringe pump. The 1 mL syringe was placed vertically, usually by taping it to a vertical surface with the tip facing downward. The chip was placed on top of the magnetic platform and was kept in place with the frame around it. An example of the prepared pre-filled system can be seen in Figure 3.16. This figure also displays a chip standard which was used to keep the chip diagonal to facilitate the prevention of air inclusions:

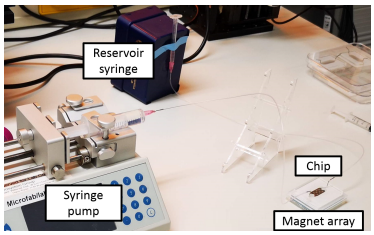

(a) *Prepared test set-up after the introduction of cell suspension*

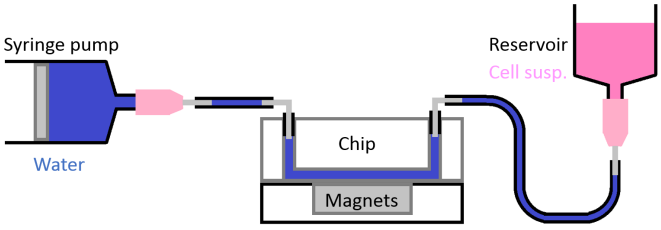

(b) *Schematic of the pre-filled test set-up*

Figure 3.16: *The test set-up as prepared right before initiation of the syringe pump.*

The MCF-7 cells were harvested when a T75 culture flask reached 80% to 95% confluence. One tenth of the cells were used for passaging to a new flask and another 10% were resuspended in 10 mL of medium (RPMI + 10% FBS + 1% P/S). This suspension was vortexed and aliquotted into two to four volumes of 1.5 mL to ensure that an initial cell count assay (through NucleoCounter NC-200) and the test (1 mL) could be easily executed. 22.5 mL of both CellSearch ferrofluid and capture enhancement agent were added to this volume of 1.5 mL.

After the initial cell-count assay, 1 mL of cell suspension was introduced into the 1 mL syringe. The desired flowrates were applied through withdrawal of the syringe pump - rather than injection - as injection required the system to also be free of air inclusions while the cells still needed to be introduced into the syringe pump. Moreover, injection of cells would have required the pump to be placed vertically in order to prevent loss of cells due to sedimentation. As such, pumping through withdrawal seemed to be the more straight-forward option. Only flowrates of 0.1, 0.3 and 1.0 mL/min were applied over the course of this research. The lower flowrate of 0.1 mL/min was chosen as the baseline as it is of the same order as the desired processing rate of 7.5 mL/hr. The upper flowrate of 1.0 mL/min was chosen as the maximum. This flowrate corresponds to a mean flow velocity of 8.33

mm/s (assuming a chamber cross section of 0.2 mm by 10 mm), which gives the cells approximately two seconds to settle inside the chamber. This should theoretically be enough time, assuming the 0.2 mm/s settling velocity calculated at the end of Section 3.1. The middle flowrate was selected as an approximated logarithmic average between 0.1 and 1.0.

The pump was stopped every time right before the last bit of fluid entered the inlet of the chip. Both lengths of tubing were detached from the isolation chamber chip and the chip was removed from the magnetic platform. The chip contained approximately 80 µL of medium, cells and CellSearch agents. The residue in the 10 mL syringe was vortexed to establish a homogeneous concentration of cells and part of the volume was subsequently deposited into a 2 mL vial for a cell-count in the NucleoCounter. Emptying the cell isolation chamber of the first measurement series as detailed in Paragraph 3.3.2 happened through careful manual ejection of the volume through a 1 mL syringe and resuspension into a vial with a known volume of water followed by vortexing and a Nucleo-Counter assay. A second chip-emptying method was attempted as well. In this case the chamber would be flushed vertically from the top downwards with 1.0 mL of de-ionized water and capturing the ejected cell suspension in a 2 mL vial, by using a 1 mL syringe pre-filled syringe. Assuming the chip, tubing and syringe were connected with negligible air inclusions, the volume collected into the vial should also be exactly 1.0 mL. The final two measurement series detailed in Paragraph 3.3.2 were executed using this method. In this case too, the extracted cells were vortexed before counting.

Each measurement series contained three tests (0.1, 0.3 and 1.0 mL/min), with each test consisting of three separate cell-count assays: 1) initial count, 2) residue count and 3) extract count. Each cell count consisted of a measured concentration and a known volume of suspension. The total cell count was obtained by multiplication of the measured concentration and the volume introduced to or extracted from the system.

3.3.2 Results

In total, three series of tests have been executed. The first two test series focused on the magnetic capture and retrieval of EpCAM+ MCF-7 cells, which were suspended in medium. The third test series was used as a negative control to confirm that no cells would remain in the isolation chamber when no magnetic field was applied. The results from this test serve as a proof of concept for EpCAM- cells that should not be bound to the CellSearch ferrofluid. All series of tests consisted of the flowrates of 0.1, 0.3 and 1.0 mL/min.

Over the course of the first test series, the cells were extracted from the chip by careful suction while keeping the chamber vertically to facilitate emptying of the chip by gravity. The cells were then resuspended into one mL of de-ionized water and counted. The measurement data can be found in Appendix Table A.2, the visualization of this data is displayed below in Figure 3.17:

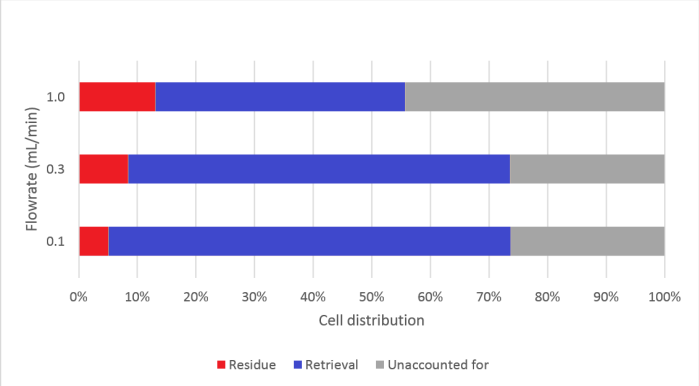

Figure 3.17: *Distribution of the retrieved cells after testing for various flowrates.*

The combined amounts of cells counted in the residue and the retrieval vials did not add up to the

amount of cells that had been introduced into the system. A reasonable explanation would be that a certain amount of cells yet remained inside either the tubing or the isolation chamber. From Figure 3.17 it follows that higher flowrates lead to a bigger loss of target cells to the residue and fewer cells retrieved in the collection vial. This corresponds with expectations, as the strong shear stress exerted by higher flowrates could drag the magnetically labelled cells across the chamber's bottom surface.

When the method of voiding the chip was changed to flushing with 1.0 mL of DI water, the unexplained loss of cells did not occur any longer. Instead, the amount of cells retrieved from the chip and the residue generally added up to more than the amount of cells injected into the system. As such, these results can only be used qualitatively, rather than quantitatively. The resulting data can be found in Appendix Table A.3. The corresponding bar chart as displayed in Figure 3.18 is normalized to 100% and it does not take the computed cell surplus into account.

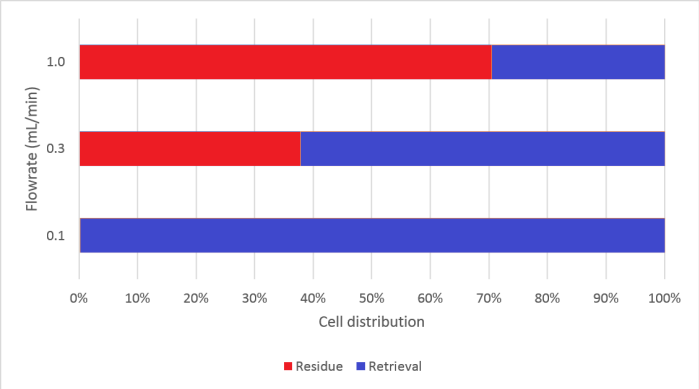

Figure 3.18: *Normalized distribution of the retrieved cells after testing for various flowrates.*

The isolation tests that were executed without the magnetic platform showed that the cells counted in the residue and retrieval vials added up to significantly more than the amount of cells counted in the initial cell suspensions, as seen in the raw data in Appendix Table A.4. In this case too, the chip was emptied by flushing with 1 mL of DI water. For that reason, this measurement series was also deemed quantitatively unreliable. The data did however qualitatively show that the MCF-7 cells were mostly found in the residue vial, rather than the retrieval vial. This made sense since the cells were not magnetically attracted towards the bottom of the chip, which should have allowed them to pass freely through the chip. The raw data found in the Appendix was again normalized to 100%. The ratio of relative amounts of captured cells in either the residue or retrieval vial can be found in Figure 3.19:

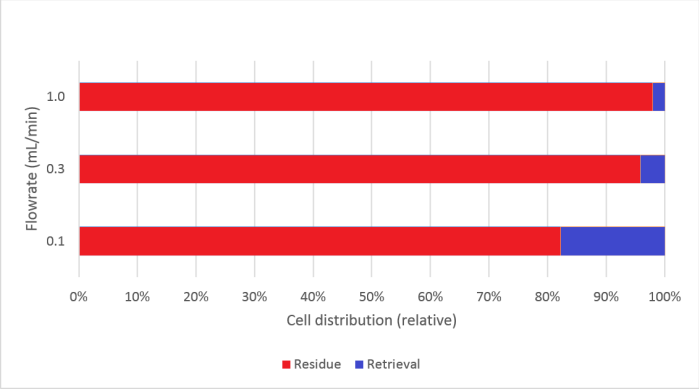

Figure 3.19: *Normalized distribution of the retrieved cells after testing without magnetic platform for various flowrates.*

4 Encapsulation

4.1 Design and fabrication

The droplet generator design used during this research is the same one as used in prior research at the Microsystems group of TU/e [Jelle J. F. Sleeboom, 2018]. The design consisted of a 2D microfluidic structure as demonstrated in Figure 2.9. The channel structures of the droplet generation part had a width of 100 µm, whereas the meandering channel towards the end of the chip had a 500 µm width. The outer dimensions of the chip were designed to fit a common microscope slide of 1" by 3". The intersection of channels where droplet generation occurs are locally narrowed to 50 micrometer, as displayed in Figure 4.1.

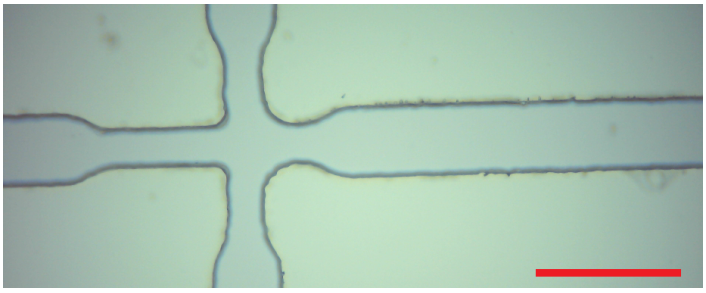

Figure 4.1: *Detailed view of the droplet generation area of the microfluidic chip. Red scale bar represents 200 µm.*

The chip was made by conventional photolithography and PDMS-casting methods. A 100 µm thick SU-8 photoresist negative image of the microfluidic chip was made on a silicon wafer by using the corresponding photomask as provided by J.J.F. Sleeboom and following the procedure of spin-coating, baking, UV-exposure and development as recommended by the photoresist's producer. The master made during this process could be re-used multiple times for casting the device halves with degassed PDMS, supplemented and mixed thoroughly with 10% crosslinking agent. The PDMS casts usually had a thickness of around 4 to 5 mm. After curing at 65 °C for at least 60 minutes, the PDMS was cut and peeled loose from the master. The inlets and outlets were punched with a 1.20 mm punch and residual PDMS debris was removed from the punched holes with pressurized nitrogen. The device halves were then either bonded to glass microscope slides or flat PDMS microslide-sized slabs after a plasma treatment with oxygen for 30 seconds at 20 W power. The bonded parts were then cured inside the same 65 °C oven for at least a day.

4.2 Methods

The fluids were delivered to the chip by mounting 1.0 mL syringes with luer-lock needles on top of separate syringe pumps. Medical grade tubing made up the connection between the PDMS droplet generation chip and the syringes via either metal syringe needles (Techcon Systems) which were bent to 90 degree angles beforehand or via pipette tips, by following the tip-loading procedure [Sinha et al., 2019]. Continuous phase consisted of mineral oil (Sigma M8410), mixed with 4 wt% Span 80 (Sigma S6760). The dispersed phase either consisted of de-ionized water or 10 µm Micromer (Micromod GmbH, Germany) ferromagnetic microparticles dispersed in de-ionized water. Special attention was paid to avoiding air-inclusions inside the syringes and the attached syringe needles and tubing. Imaging was done with an inverted microscope and videos and snapshots were taken with IC Capture 2.4 software. Flowrates in the order of microliters per minute were used over the course of this project. By applying these flowrates droplet generation occurred in the dripping regime and droplet formation and flow could clearly be visualized with the microscope.

4.3 Droplet consistency

In order to check the consistency of the generated droplets, videos were taken with the microscope and the droplet sizes were measured by image analysis. A Matlab-script was made to identify droplets by circle-detection. The script then stores all measured droplet diameters and generates a histogram with a corresponding normal distribution fit. For this specific droplet generator chip, a size distribution as displayed in Figure 4.2 was found for a dispersed flowrate of 1 µL/min and a continuous phase flowrate of 2 µL/min.

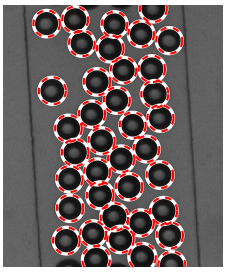

(a) *One of the frames with the detected droplets encircled.*

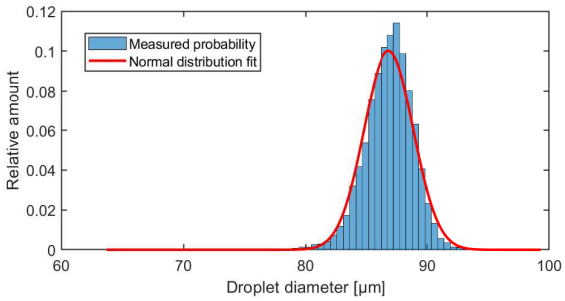

(b) *Size distribution of measured droplets.*

Figure 4.2: *Automated droplet size measurements through Matlab.*

The observed droplet sizes closely followed a normal distribution as displayed in Figure 4.2b. A mean of 86.8 µm was found with a standard deviation of 2.04 µm. The resulting dispersity was 2.4%.

4.4 Encapsulation statistics

Encapsulation of magnetic microparticles inside microfluidic droplets was explored as a means to perform simple post-encapsulation isolation tests of beads containing the magnetic particles as a model for magnetically labelled cells in order to dispose of empty beads. An isolation method such as detailed in Appendix A.7 could for example be used for this purpose. Simple loading of magnetic particles through regular tubing connection did not suffice as the density of the particles resulted in sedimentation of particles inside the tubing as the applied flowrates were relatively low. Tip-loading of the dispersed phase allowed the magnetic microparticles to steadily sediment into the chip through gravity since the fluids were introduced into the chip via vertically inserted pipette tips. Tubing and pipette tips were connected via punched PDMS plugs as demonstrated in literature [Sinha et al., 2019]. The desired concentration of Micromer 10 µm particle suspension was created by assuming one particle per 100 µm (diameter) droplet, which amounts to 1.9e3 beads per µL. This value was calculated by using Equation 2.11 The original concentration of the Micromer suspension was 8.7e4 particles per µL. The first dilution was aimed at 7.6e3 particles per µL, which was four times the desired amount, by adding 10.44 parts of DI water to the one part of the original Micromer suspension. Further dilutions of 3.8e3 and 1.9e3 particles/µL were made by 1:1 mixing of suspension and DI water.

Several attempts were made at manipulating the mean number of particles in the droplets towards desired amounts of 4, 2 and 1 particle per droplet. Clogging of the device was a major issue for the case of 4 and 2 particles per droplet, but not for the aim of 1 particle per droplet. It was observed that the initial particle contents per droplet were of the same magnitude as anticipated. As time went on, the average amount of particles contained in a droplet increased due to sedimentation, after which the contents started dropping over time, either because of clogging (2 or 4 per droplet) or because of particle depletion (1 particle per droplet). Sedimentation of particles could be visually observed by checking the tip-loaded particles as displayed in Figure 4.3a. This figure depicts how the particles

slowly settle towards the chip, creating a concentration gradient along the height of the pipette tip. Figure 4.3b displays the ferromagnetic microparticles captured inside the microfluidic droplets.

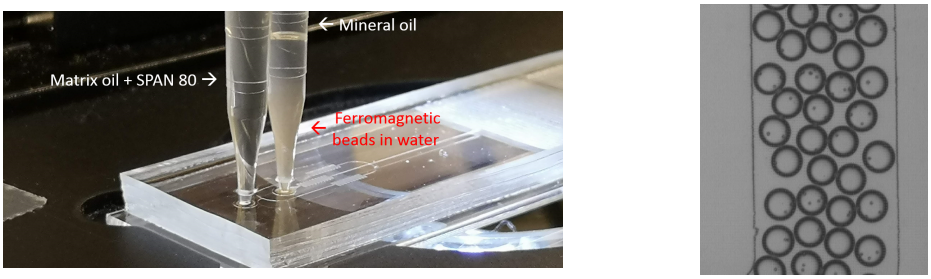

(a) *Sedimentation of tip-loaded magnetic microparticles inside the right-hand pipette tip. Approx. 15 minutes into testing.*

(b) *Droplets containing ferromagnetic microparticles.*

Figure 4.3: *Automated droplet size measurements through Matlab.*

A multitude of videos of 10 seconds have been taken during droplet generation. Subsets of these videos were analysed further through visual slow-motion inspection. The particle contents of each droplet were manually counted at a playback rate of 0.03x and a frequency distribution was made for each analysed video (blue dashed line and dots). As expected from theory, the encapsulation distributions closely resembled the Poisson distribution (Equation 2.10 fitted in red) for each 10-second video fragment as can be seen in Figure 4.4:

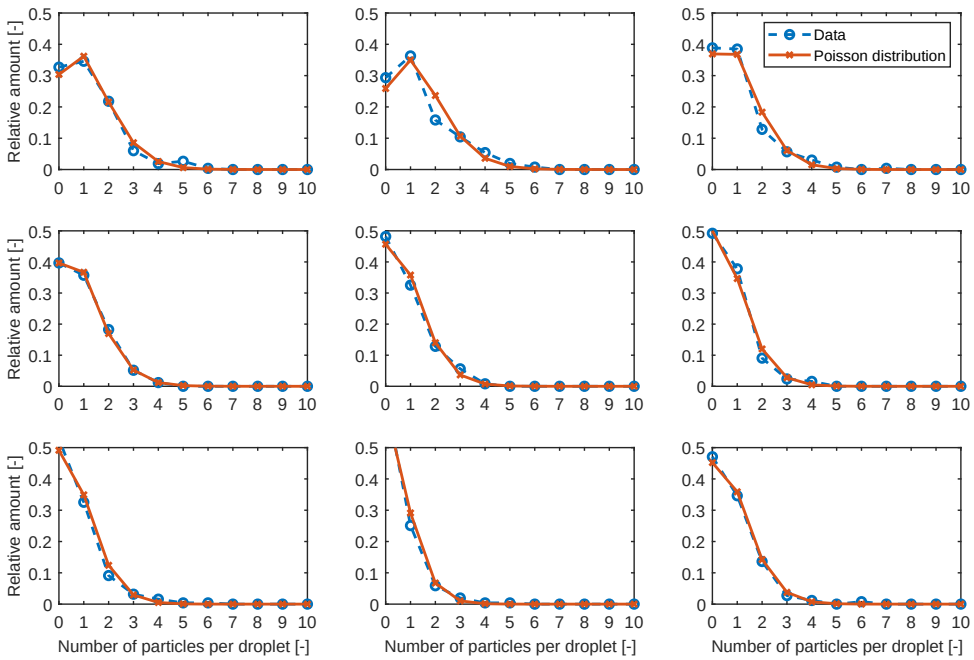

Figure 4.4: *Measured distribution and fitted Poisson distributions for nine subsequent 10-second video fragments (left to right, top to bottom). Approximately 25 minutes after droplet generation initialization. Time between first and last video fragment was 5 minutes.*

The concentration of magnetic particles was tuned in order to be 1 per 100 µm droplet. Over the course of testing, droplet contents fluctuated to a certain extent. The desired average amount of 1 particle per droplet was only achieved directly after initial droplet generation and after several minutes when droplet contents started declining again. Of course, due to Poisson statistics, consistent

encapsulation of single particles was not possible using this method. Figure 4.4 shows the observed distributions of particles over the droplets and the general decline in droplet contents over the course of five minutes, as the mean and mode generally decrease with nearly every consecutive video.

4.5 Single cell and droplet manipulation

Since the needle-in-a-haystack problem kept recurring over the course of this research, single cell manipulation methods were considered as a means to circumvent the loss of cells during mass droplet generation. This part discusses a side-track project which was aimed at injecting single cells into single droplets. This process is very similar to the intracytoplasmic sperm injection (ICSI) method, which is clinically used for the fertilization of ovum cells. A schematic detailing the concept can be found in Figure 4.5:

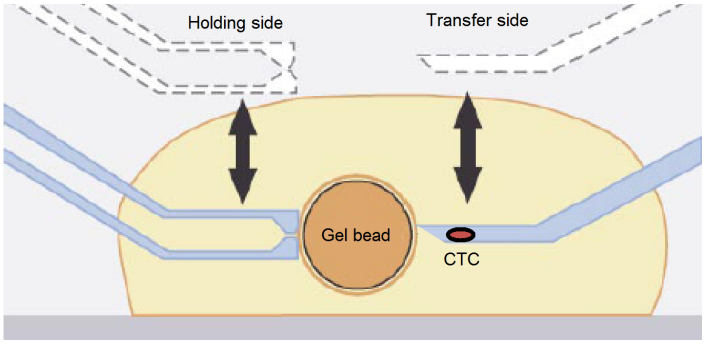

Figure 4.5: *Schematic detailing the concept of transferring a CTC into a gel bead through micromanipulation. Adaptation from an ICSI schematic (LifeInvitro).*

4.5.1 Design and fabrication

Two near-identical micromanipulators have been constructed. One was designated for cell manipulation, whereas the other manipulator was designated for the manipulation of water-in-oil droplets. One of the cell-manipulators can be seen in Figure 4.6:

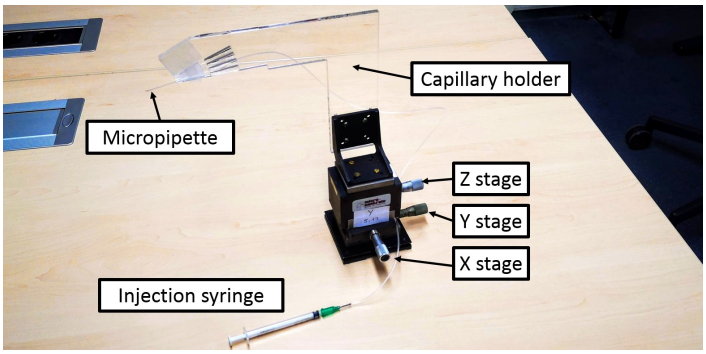

Figure 4.6: *Micromanipulator with a microcapillary mounted on top.*

Each cell-manipulator was mainly constructed with the following list of materials:

- Two horizontal micromanipulation stages for planar movement (x, y).
- One vertical micromanipulation stage for bringing the capillary into microscope focus (z).
- A 6 mm thick laser-cut PMMA micropipette holder, designed to fit the microscope.
- A 90 degree connecting piece for fastening the pipette holder to the micromanipulation stage.

- A borosilicate micropipette pulled from a capillary, connected to a 1 mL syringe via tubing.

The micromanipulators were designed for use alongside an inverted microscope with one manipulator on both sides. The three micromanipulation stages (x, y, z) were put on top of another one in such a way that the turning knobs were easily accessible (i.e. not on the microscope side of the manipulator). The horizontal bar ends with a 'head' featuring grooves which can be used for fastening the microcapillary at various angles by clamping. Clamping was done by making use of the elasticity of a laser-cut PMMA strip, which practically functioned as a leaf-spring exerting force onto the capillary. This leaf-spring was attached to the pipette holder by double sided tape. The microcapillary was attached to the 1 mL syringe via tubing and a luer-lock syringe needle.

4.5.2 System specifications

Injection micropipette tips of 30 µm outer diameter and 10 µm inner diameter were established through pulling borosilicate capillaries with a pipette puller (Sutter Instrument, U.S.A.). The same machine was used to create 100 µm outer diameter holding micropipettes for the droplets. The inner diameter of these micropipettes was reducible to 20 µm by using a microforge containing a thin filament that could be heated to locally soften the micropipette tip, leading to localized relaxation and dulling of the pipette tip.

Preliminary tests were done with solid particles to see if microparticles could be manipulated by this design. Sufficient precision movement was achieved to align the micropipettes with the 10 µm particles and to manipulate these particles by contact through the movement of the x- and y-stage of the micromanipulators and the microscope stage. Initially the micropipettes, tubing and connected syringe were pre-filled with water in order to optimize the response time of the system. However, the resulting flowrates proved to be rather high, resulting in uncontrolled flow inside the target fluid. Filling only part of the pipette tip with water while leaving most of the system filled with air allowed for more careful and gentle manipulation of particles. Surprisingly, starting and stopping injection and ejection by hand also became easier, however completely stopping flow from the micropipette was still rather difficult. An example of manipulation of small solid microparticles can be found in Figure 4.7:

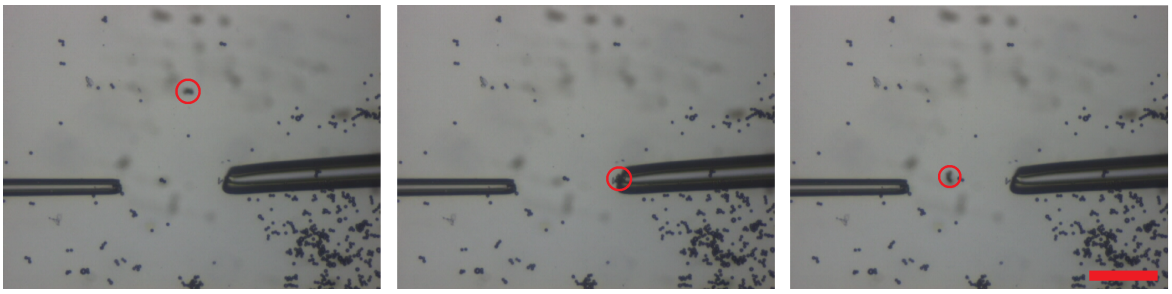

Figure 4.7: *Capture and release of a cluster of 10 µm solid particles. Red scale bar represents 200 µm.*

An attempt was made to manipulate water in oil droplets. Unfortunately, the system as demonstrated in this section was not gentle enough to the droplets. As a result, droplets were either destroyed or sucked into the capillaries. Moreover, control of the micromanipulators was rendered more difficult as gentle interactions with the desk carrying the microscope (e.g. placing elbows onto the desk) caused vibrations which were directly observed through microscope, disturbing the process. On top of that, it was rather difficult to turn the knobs of the micromanipulators without accidentally sliding the manipulator over the surface of the desk and disturbing the experiment. These practical difficulties alongside the desire for a microfluidic solution -rather than a manual one- lead to the choice to abandon further exploration of this research direction.

5 Discussion

5.1 Cell capture

5.1.1 Results

As discussed in section 3.3, the cell-counts of the cells introduced into and retrieved from the system did not add up across every experiment. Several possible explanations could be brought up to clarify this finding. During the first series of experiments, the cells were retrieved by careful manual emptying of the chamber by withdrawing a 1 mL syringe and resuspending the cells. Cells could still remain inside the chip, leading to a lower amount of cells found in the retrieval and residue vials, than initially introduced in the system. The problem reversed to counting more cells after the test than counted initially, when the method of cell retrieval was changed to flushing the chamber with exactly 1 mL of DI water. This leads to believe that flushing the chamber is more effective than extracting the cells through withdrawal of a syringe. The new errors might have been caused by error margins of the Nucleocounter for low concentrations of cells. If this is the case, this problem could for example be circumvented by manual cell counting. Another explanation could be that although cells were thoroughly aspirated before harvesting to break up cell clusters, small cell clusters still existed inside the suspension. As a result, initial assays could have contained relatively many clusters, whereas shear during tests might have reduced the concentration of cell clusters and increased the number of single cells. As a result, the amount of distinguishable cells could have increased during the latter two experiment series leading to higher counts after the test. Even though the cell count assays did not add up as expected, the general trend did show that lower flowrates lead to higher capture efficiencies. The increasing loss of cells at higher flowrates can be attributed to the shear forces that also increase for higher flowrates.

5.1.2 Prototype costs

The established microfluidic chip and magnetic array were made via a relatively simple process as demonstrated in Paragraph 3.2.3. Moreover the design of the channel and holes are relatively simple to reproduce by using other methods. An estimation of the cost of the prototypes used for this research can be found in Table 5.1:

Table 5.1: *Material cost estimation of the disposable isolation chamber chip prototypes*

Part	Material	±Cost/unit	±Cost/prt.	Source
Top	6 mm PMMA	€50/m^2	€0.10	plexiglas.nl
Middle	Double sided tape	€1/m (5cm)	€0.04	Tesa on bol.com
Bottom	125 um PMMA	N/A	negligible	Assumption thin film polymers
In-/outlet	Techcon 20 GA	€20/50pc	€0.80	Techcon Systems
Tubing	0.034” tubing	€80/30m	€1.60	Scientific Commodities
Total			**€2.54**	

The variable cost per isolation chamber was approximately €2.50. Notable mentions, however are the used Via1 cassettes (3x€2.10 per assay) used to count cell concentrations in the nucleocounter.

The magnetic platform and the frame were mostly constructed from PMMA and double sided tape as well. The neodymium magnets were purchased in a batch of 216 cubic magnets for a price of €7.10. By inserting 54 of these magnets into the magnet slot, the contribution of the magnets to the overall cost of the platform was only €1.78. The total cost of the platform prototype is estimated at €2.00 when including the PMMA and tape. Power, maintenance and operator costs of the laser cutter is not taken into account. In conclusion, the reusable magnet platform is not even as expensive as all disposables used during one test.

5.2 Encapsulation statistics

Since the target CTCs are extremely rare and microfluidic droplet generation happens at high frequency, encapsulated CTCs will likely need to be isolated from empty droplets by a second isolation step. Encapsulation of magnetic particles was explored to establish a straightforward model for droplets containing magnetically labelled cells. The number and type of particles inside a droplet determine how much force can be magnetically exerted onto the droplet of a certain size. These properties are to be tuned to resemble encapsulated magnetically labelled CTCs. For the available magnetic microparticles it was observed that tip-loading yielded the best results as it prevented settling and loss of particles inside the inlet tubing. As expected, the number of particles contained in a subset of droplets nicely followed Poisson statistics. However, the mean numbers of particles per droplet fluctuated over time since gravity caused gradual settling of the particles. This time dependent variation could be prevented by buoyancy matching the particles and continuous phase fluid. Moreover, the rather large magnetic particles used as a model for magnetically labelled cells during this research might lead to overestimation of device performance since their magnetic volume could be an overestimation of the magnetic volume of ferrofluid attached to a tumour cell. As such, magnetically labelled cells could be analyzed further and other magnetic microparticles could be considered as models better suited for magnetically labelled CTCs.

5.3 Outlook on further research

In order to work towards actual culture of cells inside beads, several adjustments to the procedure of isolation discussed in section 3.3 need to be made. Over the course of this research cell passaging was done in a sterile environment, whereas cell capture tests were done in a non-sterile environment at room temperature as the cells and chips were discarded after capture tests. In order for the cells -especially the rare and sensitive CTCs extracted from patients- to remain viable after capture and release for culture purposes, solutions need to be found to keep the cells in a sterile environment at an optimal temperature ($\pm$37 ºC). First of all, the set-up should be moved to a biosafety cabinet to minimize the risk of contamination. Secondly, the set-up should be kept heated close to body temperature. This especially holds for the chip and tubing, as the high surface to volume ratios in these parts correspond to relatively high heat dissipation to the environment at room temperature.

The method of keeping both the tubing and the device heated as demonstrated in prior work [Jelle J. F. Sleeboom, 2018] could perhaps be extended to the device and setup demonstrated in this research. Keeping the system sufficiently heated could also allow the isolation chamber to be flushed with Matrigel. This way, the captured cells can be directly resuspended in the desired culture medium. Lowering the necessary volume of medium for flushing the chamber could lead to higher concentrations of resuspended cells in the desired medium, more economical use of this medium and faster processing time of the captured cells. This method might also create an opportunity for direct connection of this isolation chamber to the droplet generation device demonstrated in the same work. If such a method were to be established, further steps to culture the tumour cells would follow directly from Sleeboom's work by embedding the CTC-Matrigel droplets in collagen and to sandwich them in-between collagen layers inside an Ibidi microslide that had premade wells as small as 4 mm in diameter as demonstrated in Figure 5.1.

If direct connection between the magnetic cell isolation chip and the droplet generator were to be established, the new challenge would be to recapture the cells inside droplets among thousands of empty microfluidic droplets. Moreover, as found during tests and discussions at Erasums UMC, plenty of leukocytes still express EpCAM to a certain degree which leads to them also being captured by the conventional CellSearch method, as well as this microfluidic method. In this case, a second isolation step would be required that can isolate the TC-containing beads from the remaining beads. Several steps towards exploring the separability of droplets containing magnetic particles were made: One of which was testing the encapsulation statistics of 10 µm magnetic microparticles (Micromod GmbH, Germany). The second one consisted of the fabrication of several types of multiple inlet, multiple outlet (MIMO) parallel flow magnetic isolation chips as outlined in Appendix A.7.2. The encapsulation statistics showed that the encapsulation of relatively high concentration

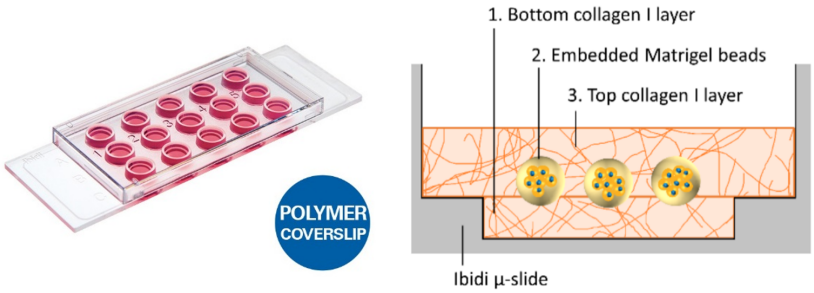

Figure 5.1: *Picture of the used wells and a schematic of MCF-7 tumour cells encapsulated in beads, embedded in collagen [Jelle J. F. Sleeboom, 2018].*

of magnetic particles showed a Poisson-like distribution. However, any attempt at making a parallel flow device, resulted either in leakage due to poor bonding (PDMS parts moulded in a micromilled PMMA mould) or showed poor resolution inside the channel, resulting in unpredictable flow. In order to establish an isolation step for droplets containing magnetic particles, straightforward methods of introducing strong magnetic fields inside microfluidic channels still deserve attention. A major issue encountered during this research was the difficulty of minimizing the distance of the permanent magnets to the microfluidic channels. Another difficulty encountered in the MIMO device was the control of flow over multiple outflow channels. The roughness of the channel due to the chosen fabrication methods seemed to influence the hydraulic resistance of the outflow channels to a significant extent. If such a device is to be established, a fabrication method needs to be found that can introduce permanent magnets as close to the channel as possible, while keeping the device waterproof and establish fine channels to allow accurate predictions for the rates of outflow due to the hydraulic resistance.

5.4 Alternative solutions

5.4.1 DEP-Array

One of the most promising solutions in the field of the rare-cell challenge might be the DEP-Array (Menarini Silicon Biosystems, Italy). This machine allows the manipulation of single cells by electrophoresis on an electrode array. The machine can identify a wide variety of cell types based on immunofluorescence and move target cells to a so-called parking area. The slogans used by this company often include the following three elements: pure, single and viable. These elements are the main topics regarding the rare-cell challenge. As such, partnering with Menarini Silicon Biosystems might be a good way to establish CTC cultures inside microfluidic droplets.

It might also be interesting for both this particular research direction and Menarini to see if microfluidic droplets can be separately moved and stored. This could perhaps prove to be a great method of isolating the relevant droplets containing tumour cells from the irrelevant empty droplets.

5.4.2 Micro manipulation

Another method of cell-sorting has also been explored over the course of this research. Micromanipulators have been used to move 10 µm microbeads with an accuracy of several micrometers with micro-pipettes. This method was based on cell insertion into an ovum in IVF procedures. The micro-pipettes were pulled with a pipette puller (Sutter Instruments Co., U.S.A). Dimensions of the injection pipette reached 10 µm inner diameter and about 25 µm outer diameter. The holder pipettes were made with a diameter of 30 µm inner diameter and 100 µm outer diameter to suit the size of the microdroplets. The pumping methods used in this research proved to be too coarse for the water in oil droplets, and as such this sidetrack was discontinued.

Professional micromanipulation devices for ICSI (intracytoplasmic sperm injection) will probably prove to be more suitable for single CTC manipulation and insertion into Matrigel droplets compared to the concept developed in this research. Although this procedure would require significant manual labor compared to the ideal microfluidic solution, it could be beneficial to use this method to circumvent the second needle-in-a-haystack problem that could be caused by mass droplet generation in conventional droplet generation devices. As such, this method of single cell manipulation deserves further attention with relation to cell culture in gel droplets.

6 Conclusions and recommendations

The final goal of ongoing research at the Microsystems group is to develop a system that can isolate, encapsulate and culture CTCs in controlled environments. In this case, these controlled environments consist of Matrigel beads. This research serves as the first steps towards establishing such a system by presenting a straightforward microdluidic chip and a corresponding magnetic platform which have been designed for the isolation of immunomagnetically labelled tumour cells from a liquid (e.g. blood). The established chip and platform were capable of isolating MCF-7 cell line tumour cells, showing higher capture efficiency for lower cell suspension flowrates. The device also showed that most of the cells could pass through the chip undisturbed when no magnetic field was applied. In this case too, more cells would be retrieved in the chip at lower flowrates. The disposable chips were also practical for transferring cells from the initial medium to another by flushing the chip with the new medium which could in the end be useful for transferring cells from patient sample to Matrigel. Both 2D and 3D models were made and simulations were done to acquire understanding of the physics behind the magnetics and to design the chip. These physics could be generalized in simple exponential and power law fitting parameters.

In terms of droplet generation, the devices made during this research could produce droplets of consistent size, with a dispersity of 2.4%. Particle encapsulation inside droplets has been tested as a means to do further research into the isolation of droplets containing magnetically labelled cells. The distributions of droplet contents showed fair agreement to the expected Poisson distributions found in droplet encapsulation statistics. The used particle contents also showed a trend of initially corresponding to the desired average amount of one particle per droplet, which was achieved by tuning the concentration of particles. These number of particles per droplet increased rapidly due to particle sedimentation into the chip and ultimately dropped below the target number of particles due to particle depletion.

An attempt was also made at micromanipulation of small particles and droplets to prevent the issue of losing cells during droplet formation. In the end, the setup was accurate enough to align micropipettes with 10 µm particles and phyiscally manipulate these particles. However the controls of the setup (both translation and pumping) were considered too coarse and sensitive to vibrations to consistently execute by hand. Moreover, this method did not meet the requirement of being a microfluidic solution to the problem. As a result, this approach was cancelled.

The isolation and loss of cells were shown qualitatively rather than quantitatively. As a result, no statistically correct statements can be made further with regards to this chip and platform. As such, the operation of this chip is still subject to further research. Moreover, an optimal flowrate to maximize isolation of target cells while minimizing capture of background cells still needs to be found. Tests with clinical samples can be considered after proper tuning of the device and test settings. As of yet, a good starting point for the flowrate could be 0.3 mL/min for this specific device geometry, since the tests showed rather large (60%) retrieval, while over 95% of the cells passed through when no magnetic field was applied. As stated before, these numbers are only an indication and not quantitatively reliable due to numbers of introduced cells and retrieved/residue cells not adding up.

The first major challenge would be to establish connectivity between the cell isolation chip and the droplet generation device through a procedure that maintains Matrigel cooled in its liquid state while being quick enough to keep the captured cells viable. A possible approach could be to design a cooling platform for the proposed chip, or by implementation of cooling on the magnetic platform. If this could be successfully implemented, the second major challenge would be to develop a method of isolating the microfluidic beads containing tumour cells. If in the end, all of these elements were to be combined successfully into a method for reliable capture and encapsulation of CTCs, this method could be a solid foundation of a clinical approach for personalized diagnostics, personalized medicine and cancer research

7 Acknowledgements

First and foremost, I would like to thank my supervisor Jaap den Toonder for his continuous support and insights over the course of this project. Without his input and connections outside of Eindhoven University of Technology, this project would not even have been possible. Also many thanks for the support from Jaco Kraan and John Martens from Erasmus UMC by allowing me to meet and do tests over there, getting a better understanding of what biological substances I was actually working with. Reading about these matters only does so much compared to actually having discussions and doing tests alongside people from the field.

I would also love to thank the supporting staff from the Microsystems group; Willie ter Elst - who retired during the time I was allowed to do my research here - , Irene Dobbelaer - Bosboom and Jaap de Hullu (Your given name has caused some confusion during your first weeks here). You were the people I could always rely on for arranging anyting I needed, be it ordering yet another roll of double sided tape, arranging my authorization for some labs or arranging the necessary trainings for using the machinery in the lab. It could all be arranged in minimal time. Thank you, Erik Homburg, for helping me take off with the magnetic simulations I needed to do to get some insights regarding the devices I was designing. You made me save quite a few hours by getting me to start off on the right track!

Special credit also goes to the people who helped me getting the practical hang of things. As I was doing a project that could be considered a spin-off or continuation of Jelle Sleeboom's tumour cell encapsulation research, it was only a matter of time before I could really need your help and insights. I really appreciated your clear and concise explanation of working with cells, as well as the discussions we had about how to approach aspects of this project.

A lot of appreciation goes out to the other members of the Microsystems group, who helped me either in a work-related way or just helped me blend in better. Andreas - who helped me start up as a TA at a bachelor's course -, James - whose wondrous stories about his youth and travels back in Zimbabwe amaze me still to this day -, Sophia - who helped me out with my first magnetic particles for tests - Plenty of thanks!

Last but not least, I especially need to thank my colleagues - and most importantly friends - from our "Schuilkeder" in Gemini Noord -1.64 with whom I had the pleasure sharing an office with. You were the people who made coming to a desolate office -nearly devoid of any sunlight- feel just like coming home. I really enjoyed our talks, discussions and games over lunch, the time spent at the basketball court and all the other times we spent together as a group outside of the University. Emma, Lucia, Matthijs, Maaike, Midia, Rathinjai, Sjors, Stuart -and towards the end of my endeavours here- Ashuya and Mahdi. You people really made the time spent here the best it could have been! I will be missing you all, but I'm sure we'll be keeping in touch and meet each other again someday.

Until then I wish you all the best of luck, wherever you may stay or end up!

Cheers, Johan.

References

[Al-Halhouli et al., 2018] Al-Halhouli, A., Al-Faqheri, W., Alhamarneh, B., Hecht, L., Dietzel, A., et al. (2018). Spiral microchannels with trapezoidal cross section fabricated by femtosecond laser ablation in glass for the inertial separation of microparticles. *Micromachines*, 9(4):171.

[Chen et al., 2017] Chen, H., Cao, B., Sun, B., Cao, Y., Yang, K., and Lin, Y.-S. (2017). Highly-sensitive capture of circulating tumor cells using micro-ellipse filters. *Scientific reports*, 7(1):610.

[den Toonder, 2011] den Toonder, J. (2011). Circulating tumor cells: the grand challenge. *Lab on a Chip*, 11(3):375–377.

[Ferreira et al., 2016] Ferreira, M. M., Ramani, V. C., and Jeffrey, S. S. (2016). Circulating tumor cell technologies. *Molecular oncology*, 10(3):374–394.

[Hoshino et al., 2011] Hoshino, K., Huang, Y.-Y., Lane, N., Huebschman, M., Uhr, J. W., Frenkel, E. P., and Zhang, X. (2011). Microchip-based immunomagnetic detection of circulating tumor cells. *Lab on a Chip*, 11(20):3449–3457.

[Jack et al., 2017] Jack, R., Hussain, K., Rodrigues, D., Zeinali, M., Azizi, E., Wicha, M., Simeone, D. M., and Nagrath, S. (2017). Microfluidic continuum sorting of sub-populations of tumor cells via surface antibody expression levels. *Lab on a Chip*, 17(7):1349–1358.

[Jelle J. F. Sleeboom, 2018] Jelle J. F. Sleeboom, Cecilia M. Sahlgren, J. M. J. d. T. (2018). Using high-throughput microfluidic single cell encapsulation to mimic the pre-invasive breast-cancer microenvironment.

[Menarini Silicon Biosystems,] Menarini Silicon Biosystems, R. The gold standard: The first and only actionable test for detecting ctcs in cancer patients, `https://www.cellsearchctc.com/`.

[Nagrath et al., 2007] Nagrath, S., Sequist, L. V., Maheswaran, S., Bell, D. W., Irimia, D., Ulkus, L., Smith, M. R., Kwak, E. L., Digumarthy, S., Muzikansky, A., et al. (2007). Isolation of rare circulating tumour cells in cancer patients by microchip technology. *Nature*, 450(7173):1235.

[Qian et al., 2018] Qian, C., Wu, S., Chen, H., Zhang, X., Jing, R., Shen, L., Wang, X., Ju, S., Jia, C., and Cong, H. (2018). Clinical significance of circulating tumor cells from lung cancer patients using microfluidic chip. *Clinical and experimental medicine*, 18(2):191–202.

[Shah et al., 2008] Shah, R. K., Shum, H. C., Rowat, A. C., Lee, D., Agresti, J. J., Utada, A. S., Chu, L.-Y., Kim, J.-W., Fernandez-Nieves, A., Martinez, C. J., et al. (2008). Designer emulsions using microfluidics. *Materials Today*, 11(4):18–27.

[Sinha et al., 2019] Sinha, N., Subedi, N., Wimmers, F., Soennichsen, M., and Tel, J. (2019). A pipette-tip based method for seeding cells to droplet microfluidic platforms. *JoVE (Journal of Visualized Experiments)*, (144):e57848.

[Sleeboom et al., 2018] Sleeboom, J. J., Amirabadi, H. E., Nair, P., Sahlgren, C. M., and Den Toonder, J. M. (2018). Metastasis in context: modeling the tumor microenvironment with cancer-on-a-chip approaches. *Disease models & mechanisms*, 11(3):dmm033100.

[Utada et al., 2007] Utada, A., Chu, L.-Y., Fernandez-Nieves, A., Link, D., Holtze, C., and Weitz, D. (2007). Dripping, jetting, drops, and wetting: The magic of microfluidics. *Mrs Bulletin*, 32(9):702–708.

[Weigelt et al., 2014] Weigelt, B., Ghajar, C. M., and Bissell, M. J. (2014). The need for complex 3d culture models to unravel novel pathways and identify accurate biomarkers in breast cancer. *Advanced drug delivery reviews*, 69:42–51.

[Zhi et al., 2019] Zhi, S., Sun, X., Feng, Z., Lei, C., and Zhou, Y. (2019). An innovative micro magnetic separator based on 3d micro-copper-coil exciting soft magnetic tips and feni wires for bio-target sorting. *Microfluidics and Nanofluidics*, 23(3):43.

A Appendix

A.1 Literature tables

Table A.1: *CTC isolation and capturing technologies*

Table 1 – CTC technologies.

Subcategory	Technology	Selection criteria	Key features	References
Immunoaffinity – Positive Enrichment *Antibodies targeting tumor-associated antigens are tethered to magnetic particles (immunomagnetic) or the device surface to capture CTCs.*				
IM	CellSearch®	EpCAM	FDA-Approved	(Cristofanilli et al., 2004; Hayes et al., 2006; Riethdorf et al., 2007)
	AdnaTest	Antibody Cocktail	CTCs captured then multiple cancer markers measured by RT-PCR	(Andreopoulou et al., 2012; Müller et al., 2012; Musella et al., 2015)
	MACS	EpCAM	Pos/Neg enrichment, high surface area to volume	(Miltenyi et al., 1990; Pluim et al., 2012)
	MagSweeper	EpCAM	High purity, can process WB, 9 mL/h throughput	(Deng et al., 2014; Kim et al., 2014; Lohr et al., 2014; Powell et al., 2012; Talasaz et al., 2009)
Microfluidic (μF) Micropost Arrays	CTC-Chip	EpCAM	Micropost array optimized for cell-antibody contacts, 1–2 mL/h	(Nagrath et al., 2007)
	GEDI	PSMA/HER2, Size	Size-based separation minimizes contamination	(Galletti et al., 2014; Kirby et al., 2012)
	OncoCEE	Antibody Cocktail	Staining procedure labels capture antibodies	(Mikolajczyk et al., 2011)
Microfluidic Surface Capture	Herringbone Chip	EpCAM	Microvortices mix sample, clusters observed, 4.8 mL/h	(Stott et al., 2010)
	GEM	EpCAM	Microvortices mix sample, 3.6 mL/h	(Sheng et al., 2014)
	Graphene Oxide Chip	EpCAM	Planar geometry, 1–3 mL/h	(Yoon et al., 2013)
	Modular Sinusoidal Microsystem (commercialized by BioFluidica)	EpCAM	Three modules: selection, impedance, and imaging, clusters observed, >86% purity, >7.5 mL/h	(Kamande et al., 2013)
Microfluidic IM	Ephesia	EpCAM	Self-assembly of magnetic μm-beads into columns, >3 mL/h	(Autebert et al., 2015; Saliba et al., 2010)
	Magnetic Sifter	EpCAM	Vertical flow configuration, 10 mL/h	(Earhart et al., 2013)
	LiquidBiopsy	Antibody Cocktail	Automated, sheath flow minimizes non-specific binding, continuous flow, 5 mL/h	(Winer-Jones et al., 2014)
μF, IM	Isoflux™	EpCAM	Automated, continuous flow	(Harb et al., 2013).
μF, IM	CTC-iChip	EpCAM, Size	Pos/neg enrichment, size-based separation debulks WB, inertial focusing aids in magnetic deflection, 8 mL/h	(Karabacak et al., 2014; Ozkumur et al., 2013)
IM, *in vivo*	GILUPI CellCollector™	EpCAM	Can process large volumes of blood	(Saucedo-Zeni et al., 2012)
Immunoaffinity – Negative Enrichment *Antibodies targeting leukocyte-associated antigens are tethered to magnetic particles or the device surface deplete unwanted background cells.*				
IM	EasySep™ Human CD45 Depletion Kit	CD45	Simple, easy-to-use batch separation	(Liu et al., 2011)
	QMS		Continuous flow, high-throughput	(Lara et al., 2004; Wu et al., 2013)
	MACS			(Giordano et al., 2012; Lara et al., 2006)
μF, IM	CTC-iChip	CD45, CD66b, Size		(Karabacak et al., 2014; Ozkumur et al., 2013)
Biophysical – Density Gradient Centrifugation *Sample placed on top of a separation medium and centrifuged to separate different cell populations based on their relative densities.*				
	Ficoll-Paque®	Density	Inexpensive, easy-to-use	(Weitz et al., 1998)
	OncoQuick	Density, Size	Porous membrane above separation media for additional separation by filtration	(Balic et al., 2005; Clawson et al., 2012; Lagoudianakis et al., 2009; Müller et al., 2005; Obermayr et al., 2010; Rosenberg et al., 2002)

Table 1 (continued)

Subcategory	Technology	Selection criteria	Key features	References
	RosetteSep™ CTC Enrichment Cocktail	Density, Antibody Cocktail	Antibody-labeling alters cell density	(He et al., 2008)
	Accucyte Enrichment and CyteSealer™	Density	Sequential density fractionation enriches target cells. Additional CyteFinder™ and CytePicker™ modules for high-throughput imaging and single-cell recovery	(Campton et al., 2015)
Biophysical – Microfiltration in Two and Three Dimensions *Size-based cell separation using pores or three-dimensional geometries.*				
2D, Track-etched	ISET®	Size, Deforma-bility	Filters fixed samples through 8-μm pores, 10–12 wells can process 1 mL each, clusters observed	(Chinen et al., 2013; Farace et al., 2011; Hofman et al., 2011; Ilie et al., 2014; Krebs et al., 2012; Pailler et al., 2013; Vona et al., 2000)
	ScreenCell®		Hydrophilic surface, fixed/live samples, 7.5/6.5-μm pores	(Desitter et al., 2011; Freidin et al., 2014)
2D, Lithography	CellSieve™		Constructed from a transparent, flexible, non-fluorescent photoresist, 7-μm pores	(Adams et al., 2014a, 2014b, 2015)
	Flexible Micro Spring Array (FMSA)		Constructed from parylene-C, can process WB, captures viable cells, clusters observed	(Harouaka et al., 2014; Kaifi et al., 2015)
3D	FaCTChecker		Constructed from parylene-C, captures viable cells between membrane layers	(Zhou et al., 2014)
	Parsortix		Viable cells released by reversing flow	
	Resettable Cell Trap		Pneumatically-controlled microvalves	(Qin et al., 2015)
	Cluster Chip		Triangular pillars designed for CTC clusters	(Sarioglu et al., 2015)
Biophysical – Inertial Focusing *Cells are passively separated by size through the application of inertial forces in microfluidic devices that affect positioning within the flow channel.*				
	Vortex	Size	No RBC lysis required, captures viable cells, easy to manufacture, clusters observed	(Sollier et al., 2014)
	ClearCell® FX		RBC lysis required, 1–1.5 mL/min, captures viable cells, easy to manufacture	(Khoo et al., 2015, 2014; Warkiani et al., 2014)
Biophysical – Electrophoresis *Separates cells based on their electrical signature using an applied electric field.*				
	ApoStream®	Electrical Signature	DEP-FFF, continuous flow, captures viable cells, >10 mL/h	(Gupta et al., 2012; Shim et al., 2013)
	DEPArray™		Requires pre-enrichment, allows recovery and manipulation of viable, single cells through DEP cages	(Carpenter et al., 2014; Fabbri et al., 2013; Fernandez et al., 2014; Manaresi et al., 2003; Peeters et al., 2013; Polzer et al., 2014)
Biophysical – Acoustophoresis *Separates cells based on acoustophoretic mobility, which is size dependent, by exposing them to acoustic waves.*				
	Acoustophoresis Chip	Size	Acoustic pre-alignment and separation	(Antfolk et al., 2015a, 2015b; Augustsson et al., 2012)

(continued on next page)

Table 1 (continued)

Subcategory	Technology	Selection criteria	Key features	References
Direct Imaging Modalities *Technologies developed to i) improve the efficiency of imaging or ii) replace enrichment through high-speed fluorescent imaging.*				
Pre-Enrichment Required	Microfluidic Cell Concentrator (MCC)	None	Passive pumping concentrates samples ~5x	(Casavant et al., 2013)
	ImageStream®	CK, CD45, DRAQ5	Hybrid of flow cytometry and fluorescence microscopy, 5000 cells/sec	(López-Riquelme et al., 2013; Zuba-Surma and Ratajczak, 2011)
Enrichment-Free	EPIC	CK, CD45, DAPI	Automated digital microscopy, clusters observed	(Marrinucci et al., 2012; Nieva et al., 2012)
	FASTCell™	CK, CD45, DAPI	Fiber-optic array allows larger field-of-view, 25M cells/min, low resolution	(Das et al., 2012; Krivacic et al., 2004; Somlo et al., 2011)
	CytoTrack	CK, CD45, DAPI	Special glass disc scanned as it spins, clusters observed, 100 M cells/min	(Hillig et al., 2015)
In vivo	Photoacoustic flow cytometry (PAFC)	Absorption spectra	Non-invasive label-free interrogation of large blood volumes	(Galanzha and Zharov, 2013)
Functional Assays *Viable CTC enrichment based on bioactivity of cells, such as protein secretion or cell adhesion.*				
	EPISPOT	Protein secretion	Discriminates between viable and apoptotic CTCs using protein secretion	(Alix-Panabières, 2012; Alix-Panabières and Pantel, 2015; Ramirez et al., 2013)
	Vita-Assay™	Cell adhesion matrix (CAM)	Enriches for viable CTCs based on preferential CAM adhesion. Clusters observed.	(Friedlander et al., 2014; Lu et al., 2010)

IM – immunomagnetic, μF – microfludic, WB – whole blood. Companies that have commercialized the technologies above are mentioned in the text.

A.2 Photographs

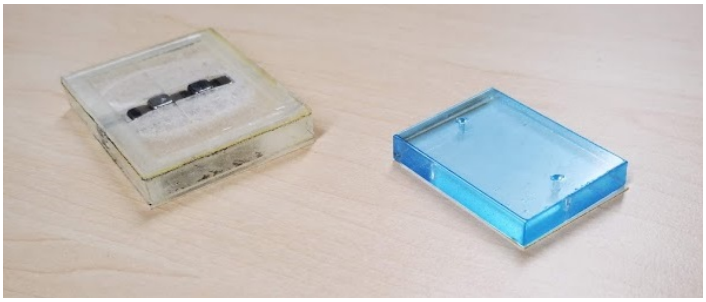

Figure A.1: *Visible relative shifting of magnets in a Halbach array kept in place in a PMMA laser-cut slot*

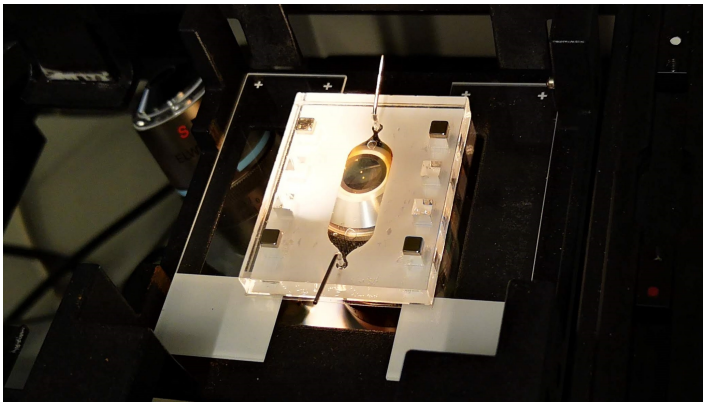

Figure A.2: *Noticable elevated concentration of ferrofluid towards the inserted magnets inside the separation chip*

A.3 Animations

The magnet array that has been modelled was reduced in size to increase the quality of the simulation. This means that periodic conditions and symmetry conditions have been applied. For the following links, only the part boxed in white has been simulated as shown in Figure A.3:

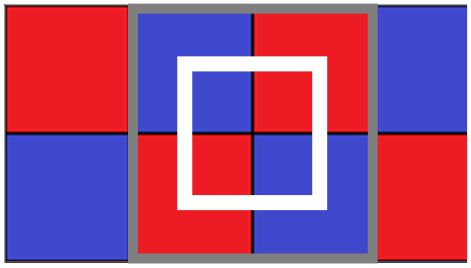

Figure A.3: *Top view of simulated part in the following simulations*

The following link shows the projection of $\nabla \vec{B}^2$ onto the plane above the magnet array at increasing height above the array: 0 to 10 seconds in the animation shows an elevation of 0 to 1 mm above the array:
`https://media.giphy.com/media/KZ9wdiddWrM7BCeog3/giphy.gif`

The following link contains an animation with the values of the component of $\nabla \vec{B}^2$ perpendicular to the magnet plane on a color scale. This animation contains four magnets as boxed in grey in Figure A.3 and also shows ten seconds of a plane going from 0 to 1 mm above the magnet surface.
`https://media.giphy.com/media/QAtEU7V6DOmfyiZetT/giphy.gif`

A.4 Figures

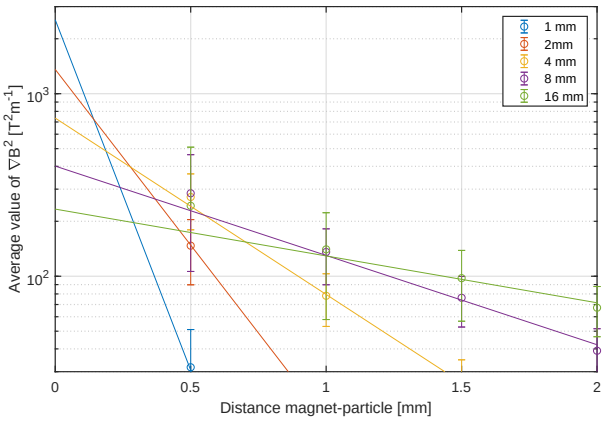

Figure A.4: *Zoom-in display of $\nabla \vec{B}^2$ for arrays of varying magnet sizes for z-values close to zero*

A.5 Protocols

A.5.1 Passaging of cells

Protocol for passaging MCF-7 cells V3

This protocol describes the procedure for passaging MCF-7 cells 1:10 to one T75 flask.

Materials	Amount (minimum)	Comments	Location
Medium	+8mL +1 mL +13mL (per flask)	RPMI + 10% FBS + 1% P/S	Fridge
PBS	+10mL		Cupboard below Hosseins setup
Trypsin	+2mL		Freezer, middle drawer, 15 mL tube
T75 flask	1		Bottom drawer next to biosafety cabinet
15mL falcon tube	1		Bottom drawer next to biosafety cabinet
P100/200/300 pipette	2		Biosafety cabinet
P1000 pipette	1		Biosafety cabinet
Pasteur pipette	-		Biosafety cabinet
Pipette boy	-		Next to centrifuge, #1 is the nicest one ☺
Centrifuge	-		Darwin room, next to small safety cabinet
Water bath	-		Darwin room, near entrance
Incubator @ 37˚C and 5% CO_2	-		Darwin room, middle one
T75 flask of MCF-7 cells	1		Incubator

1. Heat up the following in the water bath @ 37˚C for at least 30 min
    a. A 50 mL flask of Medium (if not available, make one from stock)
    b. A flask of Trypsin with at least 2mL left
2. Put 13 mL of medium in a new T75 flask and mark it with the cell type, passage number, date, and your initials. Place T75 in incubator, and medium flask back in water bath.
3. Wash the T75 flask of MCF-7 cells 2x with PBS, the general procedure is:
    a. Aspirate all liquid using a Pasteur pipette
    b. Add 5mL of PBS to the flask and slowly swivel it a few times
    c. Aspirate the PBS using a Pasteur pipette
4. Put 2mL of trypsin onto the cells and incubate for ±4 minutes
5. In the mean-time: move the warm medium from water bath to safety cabinet
6. Take a 15mL falcon tube and label for the cells (I usually only put a "C" on the cap)
7. Assess whether most cells have detached (either under the microscope, or by slight shaking and the naked eye)
8. Add 8mL of medium to the flask of MCF-7 cells to quench the trypsin
9. Using a 10mL pipette, aspirate all of the cells and medium and eject it again in the same flask (try to hit all of the flask bottom, to release the remaining cells). Repeat a second time.
10. Again aspirate the medium + cells and transfer it to the prepared 15mL falcon tube
11. Centrifuge the cells for 5 minutes at 900 rpm (**remember to use the 10mL counter-weight!**).
12. Before the centrifuge finishes, move the T75 flask to the safety cabinet (the one you left with 13mL of medium in the incubator).
13. Aspirate the supernatant medium form the cell pellet using a Pasteur pipette
14. With a P1000 pipette, add 1mL of medium to the tube
15. With a P200 pipette, aspirate and eject the cell suspension more than 30 times to re-suspend all cells.
16. With a clean P200 pipette, transfer **100 µL** of the suspension to the new T75 flask
17. While holding the T75 flask upright, swirl it a few times to spread the cells
18. Place the passaged cells in the incubator

Figure A.5: *Cell passaging protocol, as provided by J.J.F. Sleeboom*

A.6 Data

A.6.1 Cell separation

Table A.2: *Measured concentrations and calculated amounts of cells during the first test sequence, chip voided by suction*

Date	9-9-2019		Q = 0.1 mL/min		p21-p22
Test	Description	Concentration (/mL)	Original volume (mL)	Total cell count	Percentage of total (%)
1	Total count	8,24E+04	1	8,24E+04	100,0%
2	Residue	6,89E+02	6	4,13E+03	5,0%
3	Retrieval	2,83E+04	2	5,66E+04	68,7%
	Unaccounted for				26,3%
Date	16-9-2019		Q = 0.3 mL/min		p22-p23
Test	Description	Concentration (/mL)	Original volume (mL)	Total cell count	Percentage of total (%)
1	Total count	9,86E+04	1	9,86E+04	100,0%
2	Residue	1,38E+03	6	8,28E+03	8,4%
3	Retrieval	6,43E+04	1	6,43E+04	65,2%
	Unaccounted for				26,4%
Date	16-9-2019		Q = 1.0 mL/min		p22-23
Test	Description	Concentration (/mL)	Original volume (mL)	Total cell count	Percentage of total (%)
1	Total count	9,86E+04	1	9,86E+04	100,0%
2	Residue	2,14E+03	6	1,28E+04	13,0%
3	Retrieval	4,21E+04	1	4,21E+04	42,7%
	Unaccounted for				44,3%

Table A.3: *Measured concentrations and calculated amounts of cells during the second test sequence, chip voided by flushing*

Date	31-10-2019		Q (mL/min)	0,1	p24
Test	Description	Concentration (/mL)	Original volume (mL)	Total cell count	Percentage of total (%)
1	Total count	7,34E+05	1	7,34E+05	100,00%
2	Residue	6,89E+02	1,92	1,32E+03	0,18%
3	Retrieval	9,61E+05	1	9,61E+05	130,93%
	Unaccounted for				-31,11%
Date	31-10-2019		Q (mL/min)	0,3	p24
Test	Description	Concentration (/mL)	Original volume (mL)	Total cell count	Percentage of total (%)
1	Total count	5,31E+05	1	5,31E+05	100,00%
2	Residue	1,62E+05	1,92	3,11E+05	58,58%
3	Retrieval	5,12E+05	1	5,12E+05	96,42%
	Unaccounted for				-55,00%
Date	31-10-2019		Q (mL/min)	1,0	p24
Test	Description	Concentration (/mL)	Original volume (mL)	Total cell count	Percentage of total (%)
1	Total count	8,40E+05	1	8,40E+05	100,00%
2	Residue	3,22E+05	1,92	6,18E+05	73,60%
3	Retrieval	2,59E+05	1	2,59E+05	30,83%
	Unaccounted for				-4,43%

Table A.4: *Measured concentrations and calculated amounts of cells during the test sequence without magnetic platform, chip voided by suction*

Date	10-10-2019		Q = 0.1 mL/min		p22-p23 new cell batch
Test	Description	Concentration (/mL)	Original volume (mL)	Total cell count	Percentage of total (%)
1	Total count	1,08E+05	1	1,08E+05	100,00%
2	Residue	3,17E+04	3,92	1,24E+05	115,06%
3	Retrieval	2,69E+04	1	2,69E+04	24,91%
	Unaccounted for				-39,97%
Date	10-10-2019		Q = 0.3 mL/min		p22-p23 new cell batch
Test	Description	Concentration (/mL)	Original volume (mL)	Total cell count	Percentage of total (%)
1	Total count	1,06E+05	1	1,06E+05	100,00%
2	Residue	3,59E+04	3,92	1,41E+05	132,76%
3	Retrieval	6,21E+03	1	6,21E+03	5,86%
	Unaccounted for				-38,62%
Date	10-10-2019		Q = 1.0 mL/min		p22-p23 new cell batch
Test	Description	Concentration (/mL)	Original volume (mL)	Total cell count	Percentage of total (%)
1	Total count	1,03E+05	1	1,03E+05	100,00%
2	Residue	4,22E+04	3,92	1,65E+05	160,61%
3	Retrieval	3,45E+03	1	3,45E+03	3,35%
	Unaccounted for				-63,96%

A.7 Parallel flow separation

Several attempts at making a multi inflow multi outflow (MIMO) magnetic separation device were made. Such a device features (at least) two inlets and outlets with magnets aligned parallel to a microfluidic channel segment. This section outlines the various attempts at making such a device, their fabrication methods, their benefits and their shortcomings.

A.7.1 Goal

The goal of a MIMO parallel flow device was to allow selection of droplets containing magnetically labelled cells. The need for such a device arises from the combination of the principle of microfluidic droplet generation (which happens at high frequencies) and the rare cell challenge (only 1 to 10 cells/mL) would likely lead to a new needle-in-a-haystack problem. This challenge becomes even more difficult when considering that the magnetically labelled cells are bound to the same amount of CellSearch's ferrofluid, but are at the same time contained inside a droplet approximately 1000 times its volume. In order to magnetically separate magnetically labelled cells inside droplets, the magnetic properties should be optimally used. This means that the microfluidic structures and magnets should be as close as possible and flowrates should be tuned accordingly to give the encapsulated cells sufficient residence time along the magnet arrays to ensure the required lateral translation for the separation of TC-containing beads from the empty ones.

A.7.2 Designs and fabrication

The basic microfluidic concept of the devices discussed in this part are is the same as discussed in chapter 2 in Figure 2.1 [Zhi et al., 2019]. However, rather than magnetic actuation by micro-fabricated electromagnets, a passive magnetic approach was analysed over the course of this research. Initially, a design with permanent magnet arrays was planned to have magnet arrays parallel to the main channel as displayed in the mock-up design in Figure A.6:

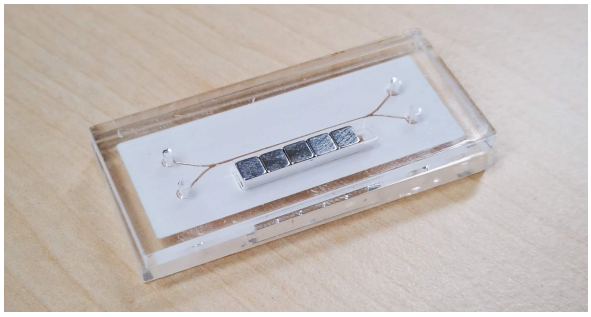

Figure A.6: *Initial design with two inlets and outlets alongside a magnet array.*

This design was made of two laser-cut PMMA plates. The top plate contained holes that were to be used as inlets and outlets, as well as a slot to contain the magnet arrays as pictured. These plates were bonded by a laser-cut piece of double sided tape. The laser-cut design within the tape contains the channels which the fluid flows through. The tape showed sufficient water resistance and strength to prevent leaking. Although this design shows the promising properties of double sided tape for this application, there were also several topics up for improvement. For instance, laser-cut double sided tape could not be cut with sufficient accuracy to establish fine channel resolution. Especially when channel direction deviated from the orthogonal degrees of freedom of the used laser-cutter, channel structures in double sided tape would be obstructed by various imperfections. These imperfections then lead to unpredictable flow characteristics inside the main channel outflow parts. Moreover, since these random imperfections also strongly influence the resistance to flow, the outflow ratios of multiple outputs is hard to tune by design as demonstrated in Figure A.7.

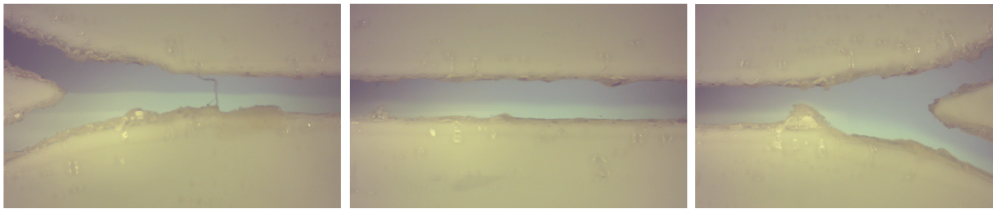

Figure A.7: *Flow behaviour within the channel structures from Figure A.6. Blue ink to water ratio of inflow 1:1, flow direction from left to right.*

These uncertainties can be reduced by using more precise fabrication procedures. Soft -lithography was explored as an alternative. For this purpose, a micro-milled mould was made as a master for the separate parts. The mould contained aligned gaps that would allow placement of magnetic arrays as close as possible to the channel. The microfluidic structure contained a channel of 1 mm wide and a distance to the boundary of 500 µm. Upon testing, it appeared that the micro-milled surface was still too coarse to allow separate PDMS-casts to properly bond despite the fine-finishing of the parts. At first glance, bonding seemed to work as desired, however when two aqueous phases were introduced to the chip leakage was observed on both sides of the chip. The structures of the leakage followed the same patterns the machine used to mill the masters, indicating that the surface-smoothing finish did not suffice.